LBL-17303
Preprint c.2

Lawrence Berkeley Laboratory
UNIVERSITY OF CALIFORNIA

RECEIVED
LAWRENCE
BERKELEY LABORATORY

MAR 14 1984

LIBRARY AND
DOCUMENTS SECTION

Submitted to Nuclear Physics A

TARGET FRAGMENT ANGULAR DISTRIBUTIONS FOR THE INTERACTION OF 86 MeV/A ^{12}C WITH ^{197}Au

R.H. Kraus, Jr., W. Loveland, K. Aleklett,
P.L. McGaughey, T.T. Sugihara, G.T. Seaborg,
T. Lund, Y. Morita, E. Hagebø, and I.R. Haldorsen

January 1984

TWO-WEEK LOAN COPY

This is a Library Circulating Copy which may be borrowed for two weeks. For a personal retention copy, call Tech. Info. Division, Ext. 6782.

NUCLEAR SCIENCE DIVISION

LBL-17303 c.2

Prepared for the U.S. Department of Energy under Contract DE-AC03-76SF00098

DISCLAIMER

This document was prepared as an account of work sponsored by the United States Government. While this document is believed to contain correct information, neither the United States Government nor any agency thereof, nor the Regents of the University of California, nor any of their employees, makes any warranty, express or implied, or assumes any legal responsibility for the accuracy, completeness, or usefulness of any information, apparatus, product, or process disclosed, or represents that its use would not infringe privately owned rights. Reference herein to any specific commercial product, process, or service by its trade name, trademark, manufacturer, or otherwise, does not necessarily constitute or imply its endorsement, recommendation, or favoring by the United States Government or any agency thereof, or the Regents of the University of California. The views and opinions of authors expressed herein do not necessarily state or reflect those of the United States Government or any agency thereof or the Regents of the University of California.

LBL- 17303

Target Fragment Angular Distributions for the Interaction of 86 MeV/A ^{12}C with ^{197}Au

R.H. Kraus, Jr.[a], W. Loveland[a], K. Aleklett[b], P.L. McGaughey[c*], T.T. Sugihara[a], G.T. Seaborg[c], T. Lund[d], Y. Morita[c‡], E. Hagebø[e], and I.R. Haldorsen[e]

Department of Chemistry
Oregon State University
Corvallis, OR 97331[a]

Studsvik Science Research Laboratory
S-611 82 Nyköping, Sweden[b]

Nuclear Science Division
Lawrence Berkeley Laboratory
University of California
Berkeley, California 94720[c]

Phillips Universität
D-3550 Marburg
Federal Republic of Germany[d]

Department of Chemistry
University of Oslo
Blindern, N-Oslo3, Norway[e]

This work was supported in part by the U.S. Department of Energy under Contract DE-AC03-76SF00098, and DE-AM06-76RL02227, Task Agreement DE-AT06-76ER70035, Mod A007, the Swedish Natural Science Research Council, the BFMT (Bonn) and the Norwegian Research Council for Science and the Humanities.

ABSTRACT

Target fragment angular distributions were measured using radiochemical techniques for 69 different fragments ($44 \leq A \leq 196$) from the interaction of 86 MeV/A ^{12}C with ^{197}Au. The angular distributions in the laboratory system are forward-peaked with some distributions also showing a backward peaking. The shapes of the laboratory system distributions were compared with the predictions of the nuclear firestreak model. The measured angular distributions differed markedly from the predictions of the firestreak model in most cases. This discrepancy could be due, in part, to overestimation of the transferred longitudinal momentum by the firestreak model, the assumption of isotropic angular distributions for fission and particle emission in the moving frame and incorrect assumptions about how the lightest ($A < 60$) fragments are produced. No evidence was found for any significant number of target fragments moving sidewise to the beam direction in apparent contradiction to the expectation of hydrodynamical model calculations. The laboratory frame angular distributions were transformed into the moving frame using various assumptions about the moving frame velocity. The resulting light fragment distributions showed an asymmetry in the moving frame indicative of their production in a fast process without the establishment of statistical equilibrium. No evidence was found for any production of the light fragments by a very asymmetric fission mechanism. The fission fragment

distributions were compared to standard formulas and an average fissioning system angular momentum of $J = 40\text{-}50\hbar$ was deduced. It was not possible to find a moving frame in which the heavy ($A > 145$) fragment distributions were symmetric about 90°.

NUCLEAR REACTIONS $^{197}Au(^{12}C,X)$ $E_{^{12}C} = 1032$ MeV; measured $d\sigma/d$ (Z,A); deduced η_{11}, fissioning system angular momentum. Intermediate energy heavy ions; firestreak model, fission, two-step model, hydrodynamical model

1. Introduction

In recent years, considerable interest has developed in characterizing nucleus-nucleus collisions in the intermediate energy regime (20-100 MeV/A). A number of studies have measured the linear momentum transfer to the target nucleus in these collisions. The situation has been characterized in a systematics of fractional momentum transfer developed by Viola et al.[1] and Stokstad et al.[2] which is shown in Figure 1. Also shown in Figure 1 are other data[3-6] which extend this correlation to higher energies. As the data of Figure 1 show, the fraction of the beam momentum transferred to the target nucleus decreases approximately linearly with increasing relative velocity of the colliding nuclei. As the projectile energy increases, incomplete fusion processes become increasingly important and it is worth noting that throughout this energy regime, the fractional linear momentum transfer significantly exceeds that observed in relativistic nuclear collisions.[3]

As informative as these measurements are, we felt that additional kinematic measurements in this energy regime would be useful in deducing the reaction mechanism(s) involved. Accordingly, we report in this paper the measurement of the target fragment angular distributions for the interaction of 86 MeV/A ^{12}C with ^{197}Au. From these measurements, we deduce a value of the average angular momentum of the fissioning system of $J = 40\text{-}50\hbar$. We show the kind of difficulties the traditional two-step model encounters in this energy region and the way in which the nuclear firestreak model fails to describe the reaction being studied.

To place this work in context of relevant previous work, one should be aware of two other areas of related work. The first of these involves

previous measurements of fragment angular distributions in nucleus-nucleus collisions at other projectile energies and with other targets. Gordon, Larsh and Sikkeland[7] measured the fission fragment angular distributions in the interaction of 7.8 and 10.3 MeV/A ^{12}C with ^{197}Au and found these distributions to be consistent with a $\frac{1}{\sin\theta}$ distribution in a moving frame corresponding to full momentum transfer. Similar findings were also made for 10.4 MeV/A ^{12}C + ^{197}Au by Viola, Thomas and Seaborg.[8] At much higher energies, Morita et al.[9] measured the target fragment angular distributions in the interaction of 3, 12 and 25 GeV ^{12}C with ^{197}Au. These four point, partial (0-90°) angular distributions were all forward peaked, with the anisotropy being larger for heavy (A > 140) fragments than for fission fragments. The data were generally consistent with the predictions of the two-step model of high energy reactions utilizing thick target-thick catcher recoil data.

In the only work done in the intermediate energy region, Blachot and coworkers[10] have measured target fragment angular distributions from the interaction of 86 MeV/A ^{12}C with ^{89}Y, ^{nat}Ag and $^{112,124}Sn$. The most dramatic of their findings was the observation of A ~ 50 fragments from the Ag and Sn targets with very high recoil energies and very strongly forward-peaked angular distributions. Blachot et al. suggested these fragments were due to quasi-compound nucleus formation followed by evaporation. However, Lund et al.[11] measured the fractional transferred linear momentum in events leading to these fragments to be 35-40% and suggested these products were the result of binary fission. Blachot et al. found the near target fragments to have strongly forward-peaked distributions which decreased exponentially with

increasing angle. They found the shapes of these distributions to be consistent with intranuclear cascade calculations.

The second major body of literature having relevance to the data presented in this paper are the many studies of target fragment angular distributions from the interaction of high energy protons with heavy targets (Au, Bi and U). Much attention in these studies has been paid to the validity of the two-step, "fast-slow" picture of high energy reactions. In reactions of 0.8-400 GeV protons with U leading to intermediate (A = 90-140) mass fragments, the observed distributions were consistent with this model.[12-14] In the interaction of 2.2 GeV protons with ^{197}Au to produce the heavy spallation product ^{149}Tb, Crespo, Cumming and Alexander[15] found the angular distributions to be consistent with the two-step model assuming a positive correlation between $v_{\parallel}$, the forward component of the velocity due to the first-step, and V, the velocity due to the second step. For the interaction of energetic protons with heavy targets to produce light fragments (A < 50), the bulk of the data suggests that the two-step model breaks down and there is no temporal separation of the production mechanism for these fragments into fast and slow steps. (In the interaction of 0.8-400 GeV protons with U to produce Sc fragments, Fortney and Porile[19] were able to find parameters within the two step model that fit their angular distributions, but they suggested that the values of these parameters were difficult to reconcile with other data on the production of these fragments.)

2. Experimental

The measurement of the target fragment angular distributions was carried out using the 86 MeV/A ^{12}C beam from the CERN SC synchrocyclotron. Two separate experiments were performed with integral particle fluxes of 2.71 x 10^{16} ions/883 min and 5.24 x 10^{16} ions/891 min, respectively. Beam fluxes were determined using Al foil monitors and the known[20] monitor cross section of 24.5 ± 3 mb for the $^{27}Al(^{12}C,X)\ ^{24}Na$ reaction. The experimental arrangement is shown in Figure 2. Two thin Au targets, one facing forward and one facing backward, were mounted perpendicular to the beam direction at the center of a cylindrical Al tube placed in an evacuated beam tube. The targets consisted of an evaporated deposit of metallic Au on a 13.4 mg/cm^2 Al backing. The backings were sufficiently thick[3] to stop any fragments from the "backward" target traveling in the forward direction and vice versa. The "forward" and "backward" Au deposits had thicknesses of 201.8 and 258.2 μg/cm^2 in the first experiment and thicknesses of 79.6 and 101.4 μg/cm^2 in the second experiment. Fragments emerging from the target were caught in 17.6 mg/cm^2 mylar ($37 \leq \theta \leq 143°$) or ~35 mg/cm^2 C foil (0-37°, 143-166°). In the second experiment, fragments emerging at angles of θ = 0-27° were caught in a "hyper-pure" C foil of thickness 33 mg/cm^2.

Following irradiation, the catcher foils were divided into ten pieces corresponding to the angular intervals of 0-14°, 14-27°, 27-37°, 37-50°, 50-63°, 63-79°, 104-124°, 124-143°, 143-153°, and 153-166°. These pieces were assayed by γ-ray spectroscopy beginning a few minutes after the end of irradiation and continuing for periods of up to 3 months in laboratories at CERN, LBL and Oregon State University. The identification of the activities

present in each foil and the calculation of cross sections from these measured activities has been described previously.[21]

The angular resolution of the experiment was dictated primarily by the angular width of the catcher foils (the beam spot size was ~4 mm^2). The alignment and centering of the beam was checked prior to the irradiation, during the irradiation and after the irradiation using radiography and on-line monitoring devices. No correction was made to the measured data for the finite angular resolution of the catcher foils because it was not felt to be critical for understanding the physics revealed by the data.

Upon analyzing the results from the first irradiation, we became aware of the large, unexpected forward angle (7°) peaks in the light ($A < 60$) fragment angular distributions. Since these angles corresponded to catcher foil segments that were struck by the beam, we became concerned about the possible effect of impurities in the C cather foils. We had, of course, irradiated blank catcher foils and found activity levels which corresponded to <2% of the measured levels (~1 ppm medium mass ($A < 100$) impurity). Nonetheless, we obtained "hyper pure" C foils (<0.02 ppm medium mass ($A < 100$) impurities) and used these foils in a second experiment to check the results of the first experiment. The results of the first and second experiments agreed in general within experimental uncertainty (generally ± 10%) and were combined to give the final results.

The biggest potential systematic difficulty with the measurements concerns the effect of target thickness and configuration upon the experimental results, principally for the heavy ($A > 120$) fragments. We shall concern ourselves with three possible effects: (a) stopping of the target

fragments in the Au deposit, (b) large angle scattering of target fragments from the Al target backing or the Au target material, (c) small angle scattering of target fragments in the Au target material. Concerning the first effect we note that the ranges of the fragments detected in this work are generally longer[3] than the value of the quantity (target thickness/cos θ) for every fragment detected in this work with the possible exception of ^{191}Pt whose range in matter is ~0.6-0.7 mg/cm^2. Even for this fragment, (and all others), a negligible fraction (<2%) of the activity found in the catcher foils was found in the target for all target thicknesses used. No difference was observed in the measured angular distributions when the target thickness was changed by over a factor of 2. Therefore it does not appear that effect (a) above was important in our measurements.

The second effect, large angle scattering of the very abundant slow, forward-moving, fragments by the thick Al target backing or the Au target could artifically elevate the observed differential cross sections at large backward angles. To evaluate the magnitude of this effect, let us consider a ^{171}Lu fragment with a kinetic energy of ~3 MeV.[3] (In an elastic collision the maximum allowed scattering angle for ^{171}Lu scattering from ^{27}Al is 9° in the laboratory system--thus we consider only the large-angle scattering for ^{171}Lu - ^{197}Au). This Lu fragment is in the velocity regime in which "nuclear" stopping is large, i.e., the velocity of the moving ion is of the order of or less than the orbital velocity of electrons in the ion. For such a case, we can use the LSS theory of scattering by Coulomb fields.[22] Let us consider their universal theory for scattering by a modified Thomas-Fermi potential.

In the LSS theory, the differential cross section for scattering through an angle θ_{CM} in the center of mass system is given as

$$\frac{d\sigma}{d\Omega} = \frac{a^2 \varepsilon^2 f(t^{1/2})}{8t^{3/2}} \tag{1}$$

where

$$\varepsilon = \langle E \rangle \frac{aM_2}{Z_1 Z_2 e^2 (M_1 + M_2)} \tag{2}$$

$$a = \frac{(4.683)(10^{-9})}{\left[Z_1^{2/3} + Z_2^{2/3}\right]^{1/2}} \quad \text{cm} \tag{3}$$

$$t^{1/2} = \varepsilon \sin\left(\frac{\theta_{CM}}{2}\right) \tag{4}$$

The quantity $\langle E \rangle$ is the recoil energy of the ion (Z_1, M_1) in the laboratory system. The stopping material is characterized by (Z_2, M_2). The relationship between θ_{CM} and θ_{lab} for an elastic collision is

$$\sin(\theta_{CM} - \theta_{lab}) = \frac{M_1}{M_2} \sin \theta_{lab} \, . \tag{5}$$

The value of the function $f(t^{1/2})$ is read from the LSS universal scattering function. Substituting in these equations the appropriate numbers for the

^{171}Lu - ^{197}Au collision, we calculate that $\frac{d\sigma}{d\Omega}$ (θ_{lab} = 90°) = 1.2 x 10^{-20} cm^2. The probability P of undergoing such a scattering is given by $nx\frac{(d\sigma)}{(d\Omega)}$ for P << 1. If we assume a path length nx of 0.2 mg/cm^2 in Au, P ≈ 0.01. Since $\frac{d\sigma}{d\Omega}$ for scattering decreases with increasing θ_{lab}, we can neglect large angle scattering at these fragment energies. Only near the end of the range will such scattering become important. (Similar conclusions to this analysis would be obtained if one considers scattering from a Bohr potential, U(r) = $Z_1Z_2e^2 \exp(-r/a')/r$, where a' = 0.53 x $10^{-8}/[Z_1^{2/3} + Z_2^{2/3}]^{1/2}$ cm.[23])

The third effect, small angle multiple scattering in the Au target, is certainly occurring. Using the LSS theory, one can calculate probabilities of small angle scattering to be 1, 0.96, 0.60 and 0.31 for ^{171}Lu - ^{197}Au collisions with θ_{lab} = 5, 10, 15 and 20°, respectively, in passing through 0.2 mg/cm^2 of Au. For the scattering of an 8.0 MeV ^{147}Eu ion[3] passing through this thickness of Au, we have scattering probabilities of 0.98, 0.32, 0.09 and 0.03 for θ_{lab} = 5, 10, 15 and 20°, respectively. For the same angles and path lengths, the scattering probabilities for an 18 MeV ^{127}Xe ion are 0.69, 0.09, 0.02 and 0.01, respectively. Thus we conclude that the measured distributions have been broadened by small angle scattering with the degree of "smearing" increasing with the fragment mass.

3. Results and Discussion

3.1. QUALITATIVE FEATURES OF THE DATA

The angular distributions for the 69 target fragments measured in this work are tabulated in Table I in the form of absolute differential cross sections. It is gratifying to note that if these absolute differential cross sections are integrated from 0 to π to obtain the total fragment production cross sections, the results are in good agreement with previous[3] thick target measurements. To simplify the discussion of these results, we have selected a representative subset of these data for a detailed analysis. The criteria for selection of the members of this subset were: (a) thick target-thick catcher recoil data[3] had to exist for the fragment, (b) the measured angular distribution had to be generally complete, with values of $d\sigma/d$ known at all angles or at enough angles to define the trend of the data. In addition, we picked fragments distributed over a wide range of A values. Figures 3-6 show the measured angular distributions for the 15 members of this subset.

A qualitative examination of the data in Figures 3-6 and Table I shows the light ($A < 60$) fragment angular distributions are strongly forward-peaked with lesser but discernible backward peaks. The light intermediate mass fragments ($60 \leq A \leq 100$) have angular distributions that are generally less forward peaked than the light fragments but have roughly similar shapes. For $A = 100$-120, the shapes of the distributions change, with the steepest portion of the distribution being from 40-100°, rather than $\theta_{lab} < 40°$. The heavy fragment ($A > 120$) distributions are very strongly forward-peaked with the degree of forward peaking decreasing for fragments near the target. One can

integrate the distributions in the angular ranges from $0-\pi/2$ and $\pi/2-\pi$ to obtain F/B ratios. The ratios so obtained have the same general trend with product mass number A as those observed in thick target-thick catcher experiments[3] but, as expected,[19] the values of F/B obtained are generally less than those measured in thick target-thick catcher experiments.

It is interesting to compare the shapes of the observed distributions with previous measurements[10] of the fragment angular distributions for the interaction of 86 MeV/A ^{12}C with ^{124}Sn. Lleres et al.[10] observed the angular distributions of products with A = 87-105 to show an exponential decrease of $\frac{d\sigma}{d\Omega}$ from about 10° to 80°. If one examines the data for products with A = 145 - 185 (roughly similar values of ΔA) for the 86 MeV/A ^{12}C + ^{197}Au reaction, one observes a similar exponential decrease from 20° to 80°. The more complete distributions of this work do show, however, that this exponential decrease does not persist beyond 80° and in fact, the distributions tend to flatten out or increase at large values of θ. For fragments with $A \geq 185$, the shapes of the distributions are changing to resemble those observed for trans-target species by Lleres et al. The sharp forward peaking observed in this work for the light fragments is generally similar to that observed for the high recoil energy ("quasi-compound nucleus") component of Lleres et al. Thus we conclude that our observations are in general agreement with previous observations involving the same projectile interacting with a medium A target like ^{124}Sn.

Comparison of the angular distribution of products with A = 147-152 from the reaction of 1.03 GeV ^{12}C with ^{197}Au with the angular distribution of A = 149 fragments from the reaction of 2.2 GeV protons with Au[15] reveals the

heavy ion reaction distribution to be very much more strongly forward-peaked. [$(F/B)_{HI} \sim 50$ while $(F/B)_p \sim 3$]. This finding is consistent with similar comparisons[24] for higher projectile energies. A similar conclusion would also follow from comparing the A = 44-60 angular distributions of this work with that of ^{24}Na produced by 2.9 GeV protons interacting with Bi[16].

Morita et al.[9] have reported crude four-point angular distributions of target fragments from the reaction of 3.0 GeV ^{12}C with ^{197}Au. For the five equivalent target fragments from both studies (^{89}Zr, ^{97}Ru, ^{145}Eu, ^{149}Gd and ^{152}Tb), one finds that the fragment distributions in this work are more strongly forward-peaked (with the possible exception of ^{89}Zr where the distribution reported in Ref. 9 has a very different shape than that reported herein, making comparisons difficult) (Figure 7).

The conclusions of this qualitative comparison of the data reported herein and other data are: (a) the qualitative changes in the fragment angular distributions with product mass number A are in agreement with previous recoil studies of this reaction (b) the general shapes of the distributions for comparable products from the 86 MeV/A $^{12}C + ^{124}Sn$ reaction are similar to those reported herein, (c) the differences between the distributions reported by us and previous work involving p-nucleus collisions are understandable in terms of the known differences between p-nucleus and nucleus-nucleus collisions, (d) the comparison between the data of this work and that of higher energy nucleus-nucleus collisions is consistent with known variations[3] of nucleus-nucleus collisions with projectile energy.

3.2. COMPARISON WITH FIRESTREAK MODEL AND HYDRODYNAMICAL MODELS

The target fragment angular distributions represent inclusive measurements that should be compared with the predictions of various phenomenological models of nucleus-nucleus collisions at intermediate energies. Data such as that of Figure 1 show that the target nucleus receives substantial momentum in the collision (i.e., is a "participant" in the reaction) and therefore the spatial distribution of these fragments after the collision has real information about the dynamics of the collision.

Loveland et al.[3] compared the predictions of three phenomenological models of intermediate energy nucleus-nucleus collisions with their data on target fragment mass distributions. For the reaction of 86 MeV/A ^{12}C with ^{197}Au, the Wilczynski generalized sum rule model[25] failed miserably to account for the observed distribution. The intranuclear cascade model of Yariv and Fraenkel[26] significantly underestimated the magnitude of both the fission and deep spallation cross sections, apparently due to an underestimation of the energy deposited by the projectile in the target nucleus. That result is not unexpected since at a projectile energy of 86 MeV/A, the wavelength of the nucleons in the projectile is not negligible with respect to the internucleon spacing in the target nucleus. Thus collective phenomena are expected to become important and these phenomena are not included in the intranuclear cascade model. Figure 1, in fact, may show evidence for substantial momentum (and mass) transfer in the collision. Lleres et al.[10] did report that their angular distributions for the 86 MeV/A $^{12}C + {}^{124}Sn$ reaction "are relatively well-fitted by the theoretical model (the Yariv and Fraenkel model) corresponding to important momentum

transfers." They also note that the fragment mass yield distribution and angular energies are reasonably described for $\Delta A \leq 25$ but not well described for $\Delta A > 25$. Because the bulk of our best data is for $\Delta A > 25$ (where small angle scattering effects are less) and because of the failure of the cascade model to describe the yields of these fragments, we choose not to compare our data to this model.

Instead we wish to compare our data with the predictions of the nuclear firestreak model.[27,28] This model gave predictions of the target fragment mass distribution in reasonable agreement with the data for the 84 MeV/A ^{12}C + ^{197}Au reaction. In this model,[27,28] the colliding nuclei are assumed to have diffuse surfaces, which were generated by folding a short-range (Yukawa) function into the conventional sharp-sphere density distribution. It was assumed that during the collision the interaction was localized to the overlap region, where collinear tubes of nuclear matter from the target and projectile underwent completely inelastic collisions. A transparency function, based upon a fixed nucleon-nucleon scattering cross-section of 30 mb, was included to prevent collisions from occurring between tubes containing an insufficient density of nucleons.

Once two tubes have collided, they are assumed to fuse and equilibrate their kinetic and thermal energies. If the resulting kinetic energy of a fused tube is less than its binding energy in the target remnant, then it is retained and contributes directly to the remnant's energy, mass, and momenta, which are explicitly conserved during the interaction.

For the reaction of 86 MeV/A ^{12}C with ^{147}Au, the primary target fragments had $194 \leq A \leq 209$, $10 \leq E^* \leq 950$ MeV, $1 \leq J \leq 84\hbar$. The "average"

fragment had A = 197.5, E* = 274 MeV, J = 26ħ and a recoil momentum of 1406 MeV/c directed along the beam axis. The deexcitation of each number of the primary fragment population was calculated using the EVA3 code[28]. EVA3 is modification of the original stepwise Monte Carlo treatment[29-31] of the deexcitation of nuclei by particle emission and fission known as the DFF code. The original DFF code was modified to include a more realistic treatment of fission competition. The excitation energy (E*) dependence of Γ_f/Γ_n is given by[32]

$$\Gamma_f/\Gamma_n = \frac{4A^{2/3}a_f(E^* - B_n)}{\left[K_0 a_n 2a_f^{1/2}(E^* - E_f)^{1/2} - 1\right]} \times \exp\left[2a_n^{1/2}(E^* - B_n) - 2a_f^{1/2}(E^* - E_f)^{1/2}\right] \tag{6}$$

where Γ_f and Γ_n are the fission and neutron emission widths, respectively, A the mass number of nucleus with excitation energy E*, neutron binding energy B_n, fission barrier height E_f, and K_0 is the rms value of the projection of the angular momentum on the nuclear axis of symmetry.

The ratio of the level density parameter at the fission saddle point, a_f, to that at the equilibrium deformation, a_n, was arbitrarily set using the relation:

$$a_f/a_n = [1 + 0.1/\log_{10}(E^* - E_f)] \tag{7}$$

The fission barrier heights are calculated using the simple approximate formula of Cohen and Swiatecki.[33]

$$E_f = 0.38(0.75 - x)E_s^0, \qquad \text{for } 1/3 \leq x \leq 2/3 \qquad (8)$$

$$E_f = 0.83(1 - x)^3 E_s^0, \qquad \text{for } 2/3 \leq x \leq 1$$

where the fissionability parameter, x is given by

$$x = \frac{Z^2}{50.88A\left(1 - 1.7826\left(\frac{A - 2Z}{A}\right)\right)^2} \qquad (9)$$

and $E_s^0 = 17.80A^{2/3}$ MeV. The variations of the widths of the fission mass distributions as a function of the Z, A, and E* of the fissioning system are calculated using the formalism of Nix.[34]

Each nucleus being deexcited was assumed to randomly emit particles in flight. If fission occurred, the fragment direction was assumed to be oriented randomly with respect to the direction of motion of the moving system.

The history of ~35,000 events was followed using the firestreak-EVA3 codes. The resulting final fragments were binned in 1 A unit wide bins and angular distributions calculated for each bin, regardless of the fragment Z. The resulting laboratory system angular distributions are shown as histograms in Figure 3-6. (The data and the calculated distribution have been normalized at 90° in Figures 3-5 and at 0° in Figure 6).

In comparing the measured calculated distributions for the light ($A < 60$) fragments, it is clear that while the predicted angular distributions are forward-peaked, they do not match in shape or magnitude the experimental data. This is not surprising since the only way to produce this class of fragments in the model calculations is by multiple particle evaporation from very highly excited nuclei or by multiple fission or by very asymmetric fission, processes which are traditionally thought of as unlikely. For the fragments with $A = 80-110$ which are part of a fission-like bump in the fragment mass distribution, the measured distributions become less forward-peaked (and progressively more fore-aft peaked) as the fragment mass number increases. The calculated distributions, however, become progressively more forward peaked as A increases. The physics behind this effect in the model is that the lower A fragments result from fission of a more highly excited species than the higher A final fragments. The more highly excited species and its fragments emit more particles which tends to smear out the angular distribution. The model has one fundamental difficulty in treating fission in this projectile energy region, i.e., it does not allow for the effect of angular momentum upon the fisson fragment angular distribution. Thus it has little chance of correctly calculating the proper fore-aft peaking in the moving frame of the fission fragment angular distribution.

For the heavier fragments ($A > 160$) the model clearly predicts a strongly forward peaked angular distribution and the measured distribution is strongly forward peaked. As discussed in Section II, small angle scattering of the fragments in the target may broaden the observed distributions so one must be careful in any comparisons we make. The crucial observation is that when we

changed the target thickness by a factor of 2.5 between the first and second experiments, the angular distributions changed $\lesssim$10% (the experimental uncertainty). (In Figure 6, the triangles and circles in the plotted ^{171}Lu angular distribution indicate the data from the first and second experiment, respectively.) From the theoretical considerations given in Section II, we conclude scattering is not playing a major role in determining the shape of the distributions. Thus it is fair to note that the calculated distribution is considerably more forward peaked than the measured distribution. A possible reason for the discrepancy between experiment and calculation is that the calculation overestimates the longitudinal momentum transfer and/or there may be significant transverse momentum transfer.

Another point of interest is the recently published[35] analysis of the ^{12}C(85 MeV/A) + ^{197}Au reaction using a full three dimensional hydrodynamical model with viscosity, thermal conductivity and final thermal breakup. Although no formal predictions of the target fragment angular distributions were made in this paper, Figure 1 of ref. 35 describing the calculations seems to show for impact parameters, b < 5 fm (~22% of the total reaction cross section), the target-like fragments are emitted sidewise. For events with b > 5 fm, the large target fragments appear to be dragged forward as the incident projectile abrades matter from the target nucleus. While the latter observation may be consistent with our data, there is no evidence for any sidewards emission in our inclusive measurements. It is important to note that the total integrated residues cross section in this work is equal to the soft spheres model[41] estimate of the total reaction cross section, arguing that we have not "missed" many (or any) fragments.

Thus direct comparison of our measured distributions with the firestreak model leads to the conclusion that the model either underestimates the transverse momentum transfer in the collision (or overestimates the longitudinal momentum transfer[3]). The hydrodynamical model calculation seems to suggest a transverse momentum transfer not observed in our data.

3.3. TRANSFORMATION OF THE ANGULAR DISTRIBUTIONS TO THE MOVING FRAME

To extract further information from the data, it was thought to be useful to transform the laboratory system angular distributions into the moving frame of the target residue following the initial projectile-nucleus encounter. We assume that the final velocity of the fragment in the laboratory system can be written as $\vec{v}_\ell = \vec{V} + \vec{v}$ where the velocity $\vec{v}$ is the velocity of the moving frame and $\vec{V}$ is the velocity kick given the target fragment by fission or particle emission at an angle θ_{MF} with respect to the beam direction in the moving frame. The vector $\vec{v}$ has components of $v_\parallel$ and $v_\perp$ parallel and perpendicular to the beam direction. In lieu of detailed information about $v_\perp$, the general strong forward-peaked nature of the distributions, and the difficulty of obtaining information about $v_\perp$, we have assumed $v_\perp = 0$. We have used standard formulas[36] to make laboratory to moving frame transformations for $\frac{d\sigma}{d\Omega}$ and θ. For the value of $\eta_\parallel$ $(= v_\parallel/V)$ needed to make such transformations, we have used three different values: (a) $\eta_\parallel$ as derived from the thick target-thick catcher experiments[3] where $\eta_\parallel^{37} = \langle \frac{v_\parallel}{V} \rangle$ (b) $\eta_\parallel$ as derived from integrating our angular distributions where $\eta_\parallel = (F-B)/(F+B)$. (c) The "best fit" of $\eta_\parallel$ as judged by the requirement that the transformed distribution be symmetric about

90° in the moving frame. The results of these transformations are shown in Figures 8-10.

Certain features of the data of Figures 8-10 stand out. With the exception of ^{74}As and ^{87}Y, the use of single, average $\eta_{\parallel}$ values from thick target experiments[3] does not lead to proper symmetrization of the angular distributions. Furthermore, from examining the data of Figs. 8-10, it is clear that if one parameterizes the moving frame angular distributions as $W(\theta_{cm}) = \frac{a + b\cos^2\theta}{a + b/3}$, then in no case is $\frac{b}{a} = 0$ as assumed in the thick target-thick catcher data analysis procedure.[37] This conclusion can also be seen by examining the data of Figures 3-6 in which the measured laboratory angular distributions are compared with those calculated from the formula[12]

$$F_L(\theta_L) = \frac{1 + (b/a)\cos^2\left[\theta_L + \sin^{-1}(\eta_{\parallel}\sin\theta_L)\right]}{1 + b/3a} \times \frac{\left[\eta_{\parallel}\cos\theta_L + \left(1 - \eta_{\parallel}^2\sin^{-2}\theta_L\right)^{1/2}\right]^2}{\left(1 - \eta_{\parallel}^2\sin^2\theta_L\right)^{1/2}} \tag{10}$$

where $b/a = 0$ and $\eta_{\parallel}$ is taken from ref. 3. In general there is poor agreement between the data in Figures 3-6 and the predictions of equation 10.

We have also transformed the data from the laboratory to the moving frame using a distribution of $\eta_{\parallel}$ values (appropriate to the thick target experiment formalism[37]) rather than a single average value $\eta_{\parallel}$. The resulting angular distributions were as asymmetric in the moving frame as those obtained using a single value of $\eta_{\parallel}$ for the transformation.

The significance of these observations remains to be determined. Strictly speaking, thick target-thick catcher recoil measurements give range-weighted measures of $\eta_{\parallel}$, i.e., $\frac{\langle \eta_{\parallel} R \rangle}{\langle R \rangle}$, where R is the range of the recoiling target fragment in the target material. If one assumes $v_{\parallel}$ is not a function of V, one can calculate[37] $\langle v_{\parallel}/V \rangle$ from the measured data. Winsberg states[37] that $\eta_{\parallel}$ calculated from such a formalism should be equivalent to that calculated from thin-target data. But the two values of $\eta_{\parallel}$ are not equivalent for this experiment. In fact, from the data of Figures 8-10 (and Figures 3-6) it would appear that the thick target-thick catcher data analysis procedure generally leads to erroneous values of $\eta_{\parallel}$. Yet one can note that the values of $v_{\parallel}$ and V derived from such an analysis[3] for fission fragments in the 86 MeV/A $^{12}C + {}^{197}Au$ reaction are in good agreement with those measured using other techniques.[1,5] It is difficult therefore to reconcile these observations about thick target-thick catcher experiments.

The second observation about the data in Figures 8-10 is that the use of η derived from thin target experiments, $\eta_{\parallel}^{\theta}$, appears to lead to a proper symmetrization of the fission fragment ($74 \leq A \leq 111$) distributions in the moving frame. For the light fragments ($A < 60$) the use of $\eta_{\parallel}^{\theta}$ does not properly symmetrize the distributions with the extent of such failure increasing as the fragment mass decreases. The most dramatic effect is for the heavy ($A > 147$) fragments where no choice of $\eta_{\parallel}$ (in the range $-1 \leq \eta \leq 1$) gives a moving frame distribution that is symmetric about 90°. This latter observation could be the result of: (a) a single "fast" reaction mechanism for the production of these fragments (which would not permit the separation of the reaction into two temporal stages ("fast" and "slow") leading to the

requirement of symmetry about 90° in the moving frame) <u>or</u> more likely (b) fundamental difficulties in transforming to a moving frame for high $\eta_{\parallel}$ values. The transformations of the distributions from the laboratory to the moving frame assume $\eta_{\parallel}$ is single valued. The heavy fragment events observed at backward angles in the laboratory system probably result from the tail of the real $\eta_{\parallel}$ distribution in which V is large or events in which the scattering has occurred. Such events are not properly transformed by an average $\eta_{\parallel}$ value and may be the source of unusual peak in the moving frame distribution for the angular range 160-180°. But the rest of the distribution (0-160°) is not symmetric either. A value of $\eta_{\parallel} > 1$ would be required to attempt to symmetrize the portion of the distribution in the range 0-160°. But if $\eta_{\parallel} > 1$, there is no unique relationship between angles, solid angles, etc. in the laboratory and moving frame and no transformation is possible without information about $\frac{d^2\sigma}{d\Omega dE}$ (b) rather than just $\frac{d\sigma}{d\Omega}$ (θ).

What can we conclude from our effort to transform the heavy fragment distributions into a moving frame? In view of the large asymmetries in the moving frame distributions using values of $\eta_{\parallel}$ derived from thick target measurements it seems safe to remark that reliable information about the properties of these fragments cannot be obtained from thick target measurements. The more fundamental question about whether the production mechanism for these fragments is "fast" or involves both "fast" and "slow" steps cannot be answered just using the data reported herein. We should note tha the spallation product energy spectra measured by Lleres <u>et al</u>. for the reaction of 86 MeV/A ^{12}C with ^{124}Sn appear to be Maxwellian in character supporting the idea of a "fast-slow" mechanism. We can say, however, if the reaction can be separated into two temporal stages, then $\langle\eta_{\parallel}\rangle > 1$.

As discussed previously, the fission fragment ($74 \geq A \geq 111$) distributions appear to be relatively well behaved. From the data in Figure 9, one can see that, in general, the moving frame distributions do not have the shape frequently used to describe the fragment angular distributions from low energy, low angular momentum fission, i.e.,

$$W_{(\theta_{MF})} = a + b \cos^2 \theta_{MF} \tag{11}$$

Instead the distribution shapes are more like those observed for fission of a system with moderate to high angular momentum.[7,8] Huizenga et al.[38] have shown that the angular distribution of an excited fissioning system with angular momentum J (and projection on the beam axis M=0) can be written as

$$W^J_{M=0}(\theta) = \frac{\left(\frac{\pi}{2}\right) (2J+1) \exp\left[-(J+1/2)^2 \sin^2 \theta/4K_0^2\right] J_0\left[i(J+1/2)^2 \sin^2\theta/4K_0^2\right]}{2\pi(\pi^{1/2}/2)(2K_0^2)^{1/2} \operatorname{erf}\left[J+1/2)/(2K_0^2)^{1/2}\right]} \tag{12}$$

where J_0 is the zero order Bessel function with an imaginary argument, and erf $[J+1/2)/(2K_0^2)]$ is the error function defined by

$$\operatorname{erf}(x) = \left(\frac{2}{\pi^{1/2}}\right) \int_0^x \exp(-t^2)dt \tag{13}$$

K_o^2 is the mean square projection of J upon the nuclear symmetry axis. For a Fermi gas, K_o^2 is given as

$$K_o^2 = \frac{I_{rigid}T}{\hbar^2} \tag{14}$$

where I_{rigid} is the rigid body moment of inertia of the fissioning system and T is its temperature. To use equation (12) to calculate the moving frame fission fragment angular distribution, we would need to know the J and E* distributions for each fissioning system, K_o^2 for each system and be assured that M=0 along with appropriate averages over all fissioning systems. None of these conditions are fulfilled in the present case. However, equation (12) can be used, with certain assumptions to make a crude, "ball-park" estimate of the average angular momentum of the "average" fissioning system in the reaction under study.

If we assume an average fissioning system excitation energy of ~600 MeV[3], use the relations $E^* = aT^2 - T$ and $I_{rigid} = 2/5\ r_o^2 A^{5/3}$ with $r_o = 1.25$ fm and $a = A/10$, then we calculate $K_o^2 \sim 444$. Using equations 12 and 13, we fit the moving frame angular distributions of the fission fragments to extract a best fit value of J, i.e., $\langle J \rangle = 40 - 50\hbar$. These estimates can be compared to the firestreak model calculations for the "average" fissioning system of $E^* = 735$ MeV and $J = 55\hbar$. As with the "average" fragment, the firestreak model seems to predict a "harder" collision than actually occurs.

For light fragment distributions in the moving frame (Figure 8), one observes that $\eta_{\parallel}^{\theta}$ is substantially greater (~2x) than $\eta_{\parallel}$ deduced from thick target results[3] and neither choice properly symmetrizes the distribution. These observations would be consistent with a failure of the two step model for the processes leading to light fragment production or possibly the existence[16] of an anticorrelation between $v_{\parallel}$ and V. Because of the strongly forward peaked character of the angular distributions, it is very difficult to measure velocity spectra at backward angles and thus check the possibility of anticorrelations between v and V. However, an independent determination of the proper value of η to use in the transformation can be found in the work of Lynen et al.[4]. Lynen et al. determined the moving frame velocity for these light fragments to be ~0.012c. From the published velocity spectra for Z=9 and Z=15 fragments, we can extrapolate a value of V ~ 0.047 for Z=21 fragments, giving $\frac{\langle v_{\parallel}\rangle}{\langle V\rangle} = 0.26$ for Sc fragments, which is similar to that derived from thick target-thick catcher measurements,[3] where $\frac{\langle v_{\parallel}\rangle}{\langle V\rangle} = 0.25$ ($\eta_{\parallel} = \langle \frac{v_{\parallel}}{V} \rangle = 0.31$). Thus it would seem that the proper choice of $\eta_{\parallel}$ is 0.31 and the angular distribution of these light fragments is not symmetric in the moving frame, indicating the lack of a two step mechanism for the production of these fragments.

Lynen et al.[4] did show that the light fragments were produced in a binary breakup mechanism. Some years ago, Moretto[39] suggested a possible mechanism for the production of light fragments by very asymmetric fission like decay of an excited nucleus. Evidence for the occurrence of this process in the reaction of 90 MeV ^{3}He with Ag has been reported.[40] The signature for the occurrence of this process is the increasing anisotropy of the

fragment angular distributions as the fragment mass increases. Lynen *et al.*[4] deduce just the opposite behavior for the lighter elements from the shifts in velocity spectra with angle. If we assume a constant moving frame velocity for the fragments with $44 \leq A \leq 59$, then we can use the laboratory frame distributions as a measure of the variation of the anisotropy with fragment mass. Figure 11 shows two measures of the anisotropy, $\frac{d\sigma}{d\Omega}(7^\circ)/\frac{d\sigma}{d\Omega}(114^\circ)$ and $\frac{d\sigma}{d\Omega}(160^\circ)/\frac{d\sigma}{d\Omega}(114^\circ)$ and their variation with fragment mass number. There is no clear trend of decreasing anisotropy with increasing fragment mass. Thus we conclude that this mechanism for producing light fragments is not playing a dominant role in the interaction of 86 MeV/A ^{12}C with ^{197}Au.

IV. Summary and Conclusions

What have we learned about target fragment production in the reaction of 86 MeV/A ^{12}C with ^{197}Au from this work and that of others? Let us divide the fragments into three classes, light ($A < 60$), fission ($75 \leq A \leq 110$) and heavy fragments ($A > 140$) as we try to answer this question.

The mechanism for light fragment production has been reported previously to be binary in character.[4] The process involved is "fast," i.e., there is not enough time to establish statistical equilibrium in the moving frame. The dominant process is not a very asymmetric fission.

The "average" fissioning system has an excitation energy of ~600 MeV[3] and an angular momentum of 40-50$\hbar$. The nuclear firestreak model coupled with th EVA3 deexcitation calculation approximately describes this group of nuclei in that it can predict[3] the shape of the fission mass distribution and it predicts the average fragment excitation energy and angular momentum within 25%.

The production of heavy fragments is traditionally thought of as proceeding via a "spallation" mechanism, with separation of the reaction into fast and slow stages. If this is the case, the average momentum transfer to these nuclei in the fast stage of the reaction is greater than the average vector sum of any random momentum kicks given these fragments during the slow stage of the reaction. Alternatively the mechanism could involve a single fast step. The dissimilarity in the angular distributions, the yields[3], and the velocities of the moving frame would indicate that these fragments are not primarily formed as the complement of the light fragments. The nuclear firestreak model overestimates the longitudinal momentum transfer leading to these events.

No evidence is seen for significant numbers of sidewise moving target fragments as might be expected from a crude evaluation of the predictions of hydrodynamical models.

The traditional method of making survey measurements of the kinematic properties of target fragments, the thick target-thick catcher method, contains assumptions about the angular distributions of the fragments that are not generally consistent with our data. The method seems to be inappropriate for extracting the kinematic properties of the heavy fragments with strongly forward peaked angular distributions. Despite the seemingly inadequate treatment of the fragment angular distributions and the fundamental inadequacy of the two step model for light fragments, the average kinematic properties of the light and fission fragments extracted using this method are in reasonable agreement[3,4] with those measured using other techniques.

Acknowledgment

This work was supported in part by the U.S. Department of Energy under Contract DE-AC03-76SF00098, and DE-AM06-76RL02227, Task Agreement DE-AT06-76ER70035, Mod A007, the Swedish Natural Science Research Council, the BFMT (Bonn) and the Norwegian Research Council for Science and the Humanities. We gratefully acknowledge the assistance of the SC synchrocyclotron operations staff and the CERN health physics staff, the members of the ISOLDE collaboration and Mr. K.J. Moody in making these measurements. Special thanks should go to Dr. Per Hoff for counting the irradiated samples at CERN.

References

*Present address: Los Alamos National Laboratory, Los Alamos, NM 87545

‡Present address: UCSF, San Francisco, CA

1. V.E. Viola, Jr., B.B. Back, K.L. Wolf, T.C. Awes, C.K. Gelbke, and H. Breuer, Phys. Rev. C26 (1982) 178; V.E. Viola, Jr., R.G. Clark, W.G. Meyer, A.M. Zebelman, and R.G. Sextro, Nucl. Phys. A261 (1976) 174.
2. R.G. Stokstad, Y. Chan, M. Murphy, I. Tserruya, S. Wald and A. Budzanowski, Lawrence Berkeley Laboratory Report LBL-15874, (1983).
3. W. Loveland, K. Aleklett, P.L. McGaughey, K.J. Moody, R.M. McFarland, R.H. Kraus, Jr., and G.T. Seaborg, Phys. Rev. C (submitted for publication).
4. U. Lynen, H. Ho, W. Kuhn, D. Pelte, U. Winkler, W.F.J. Moller, Y.T. Chu, P. Doll, A. Gobbi, K. Hildenbrand, A. Olmi, H. Stelzer, R. Bock, H. Lohner, R. Glasow and R. Santo, Nucl. Phys. A387 (1982) 129c.
5. J. Galin, H. Oeschler, S. Song, B. Borderie, M.F. Rivet, I. Forest, R. Bimbot, D. Gardes, B. Gatty, H. Guillemot, M. Lefort, B. Tamain, and X. Tarrago, Phys. Rev. Lett. 48 (1982) 1787; M.F. Rivet, B. Borderie, S. Song, D. Guerreau, H. Oeschler, R. Bimbot, I. Forest, J. Galin, D. Gardes, B. Gatty, M. Lefort, B. Tamain, and X. Tarrago, Nucl. Phys. A387 (1982) 143c.
6. G. Nebbia, E. Tomasi, C. Ngo, X.S. Chen, G. LaRama, S. Leray, P. Lhenoret, R. Lucas, C. Mazur, M. Ribag, C. Cerruti, S. Chiodelli, A. Demeyer, D. Guinet, J.L. Charvet, M. Morjian, Y. Pranal, A. Peghaire, L. Sinopoli, J. Uzureau, and R. de Swiniarski, Z. Phys. A311 (1983) 247.

7. G.E. Gordon, A.E. Larsh and T. Sikkeland, Phys. Rev. 118 (1960) 1610; Phys. Rev. 120 (1960) 1341.

8. V. Viola, T.D. Thomas and G.T. Seaborg, Phys. Rev. 129 (1963) 2710.

9. Y. Morita, W. Loveland, P.L. McGaughey and G.T. Seaborg, Phys. Rev. C26 (1982) 511; Y. Morita, W. Loveland and G.T. Seaborg, Phys. Rev. C (to be published).

10. J. Blachot, J. Crancon, J. Genevey, A. Gizon and A. Lleres, Z. Phys. A301 (1981) 91; J. Blachot, J. Crancon, H. Nifenecker, A. Lleres, A. Gizon, and J. Genevey, Z. Phys. A303 (1981) 85; A. Lleres, J. Blachot, J. Crancon, A. Gizon and H. Nifenecker, Z. Phys. A312 (1983) 177.

11. T. Lund, D. Molzahn, B. Bergerson, T. Bjornstad, E. Hagebo, I.R. Haldorsen, C. Richard-Serre and the ISOLDE collaboration, Phys. Lett. 116B (1982) 325.

12. N.T. Porile, S. Pandian, H. Klonk, C.R. Rudy, and E.P. Steinberg, Phys. Rev. 19 (1979) 1832.

13. S. Pandian and N.T. Porile, Phys. Rev. C23 (1981) 427.

14. V.P. Crespo, J.B. Cumming and A.M. Poskanzer, Phys. Rev. 174 (1968) 1455.

15. V.P. Crespo, J.B. Cumming and J.M. Alexander, Phys. Rev. C2 (1970) 1777.

16. J.B. Cumming, R.J. Cross, Jr., J. Hudis and A.M. Poskanzer, Phys. Rev. 134 (1964) B167.

17. A.M. Poskanzer, G.W. Butler and E.K. Hyde, Phys. Rev. C3 (1971) 882.

18. D.R. Fortney and N.T. Porile, Phys. Rev. C22 (1980) 670.

19. D.R. Fortney and N.T. Porile, Phys. Rev. C21 (1980) 2511.

20. J.W.N. Tuyn, R. Deltenre, C. Lamberet, and G. Rowland, CERN Technical Memorandum HS-RP/TU/80-5 (1980).

21. D.J. Morrissey, D. Lee, R.J. Otto and G.T. Seaborg, Nucl. Instr. Meth. 158 (1978) 499.

22. J. Lindhard, M. Scharff, and H.E. Schiott, Kgl. Danske Videnskab. Selskab, Mat.-Fys. Medd. 33 (1963) No. 14.

23. E. Everhart, G. Stone and R.J. Carbone, Phys. Rev. 99 (1955) 1287.

24. W. Loveland, D.J. Morrissey, K. Aleklett, G.T. Seaborg, S.B. Kaufman, E.P. Steinberg, B.D. Wilkins, J.B. Cumming, P.E. Haustein and H.C. Hseuh, Phys. Rev. C23 (1981) 253.

25. J. Wilczynski, K. Swiek-Wilczynska, J. van Driel, S. Gonggrijp, D.C.J.M. Hageman, R.V.F. Janssens, J. Lukasiak, and R.H. Siemssen, Phys. Rev. Lett. 45 (1980) 606.

26. Y. Yariv and Z. Fraenkel, Phys. Rev. C20 (1979) 2227.

27. W.D. Myers, Nucl. Phys. A296 (1978) 177.

28. P.L. McGaughey, Lawrence Berkeley Laboratory Report LBL-15325, (1982).

29. I. Dostrovsky, P. Rabinowitz, and R. Bivins, Phys. Rev. 111 (1958) 1695.

30. I. Dostrovský, Z. Fraenkel and P. Rabinowitz, Proc. 2nd UN Int'l Conf. Peaceful Uses of At. Energy, 15 (1958) 301.

31. I. Dostrovsky, Z. Fraenkel, and G. Friedlander, Phys. Rev. 116 (1959) 683.

32. R. Vandenbosch and J.R. Huizenga, Nuclear Fission (Academic, New York, 1973) p. 233.

33. S. Cohen and W.J. Swiatecki, Ann. Phys. NY 22 (1963) 406.

34. J.R. Nix, Nucl. Phys. A130 (1969) 241.

35. G. Buchwald, G. Graebner, J. Theis, J.A. Maruhn, W. Greiner and H. Stocker, Phys. Rev. C28 (1983) 1119.

36. J.B. Marion, T.I. Arnette and H.C. Owens, Oak Ridge National Laboratory Report ORNL-2574 (1959).

37. L. Winsberg, Nucl. Instrum. Methods, 150 (1978) 465.

38. J.R. Huizenga, A.N. Behkami and L.G. Moretto, Phys. Rev. 177 (1969) 1826.

39. L.G. Moretto, Nucl. Phys. A247 (1975) 211.

40. L.G. Sobotka, M.L. Padgett, G.J. Wozniak, G. Guarino, A.J. Pacheco, L.G. Moretto, Y. Chan, R.G. Stokstad, I. Iserruya and S. Wald, Lawrence Berkeley Laboratory Report LBL-15696, (1983).

41. P. J. Karol, Phys. Rev. C11 (1975) 1203.

Figure Captions

Figure 1. Fraction of beam momentum transferred to target nucleus in nucleus-nucleus collisions leading to fission or residue production as a function of the relative velocity of the colliding ions. Filled circles are data from Ref. 1 and 2, open circles--Ref. 3, filled triangles--Ref. 4, squares--Ref. 5, open triangles--Ref. 6.

Figure 2. Schematic diagram of the experimental apparatus used in measuring the target fragment angular distributions. The target foil dimensions have been expanded to show details.

Figure 3. Measured target fragment angular distributions from the interaction of 86 MeV/A ^{12}C with ^{197}Au. The solid lines are to guide the eye through the data, the histograms represent predictions of the nuclear firestreak model while the dashed lines represent the two-step model predictions with b/a = 0 and $\eta_{\parallel}$ taken from Ref. 3.

Figure 4. See Figure 3 for description.

Figure 5. See Figure 3 for description.

Figure 6. See Figure 3 for description. See text for discussion of additional points in ^{171}Lu graph.

Figure 7. Comparison of target fragment angular distributions for the ^{12}C + ^{197}Au reaction (solid circles--86 MeV/A ^{12}C; open circles, 3 GeV/A ^{12}C--Ref. 9).

Figure 8. Angular distributions of V, the kick given the primary target fragment by fission or particle emission, in the moving frame for fragments with $46 \leq A \leq 76$. The solid points (solid line) result from using thick target recoil data for $\eta_{\parallel}$, solid triangles represent $\eta_{\parallel}$ from thin target data while the open circles (dashed line) are a "best fit" to the data. For ^{74}As, the "best fit" and thin target data are the same as the thick target data.

Figure 9. Same as Figure 8 except $83 \leq A \leq 103$. For ^{87}Y, ^{95}Zr, ^{99}Mo and ^{103}Ru, the thin target data are the best fit, also shown for comparison are the shapes of $a + b \cos^2 \theta$ distributions that resemble the data.

Figure 10. Same as Figure 8 execpt $111 \leq A \leq 191$. For ^{111}In, the thin target data are the best fit and are equivalent to the thick target data. For the rest of the nuclides, there are no "best fit" curves since no choice of η seemed to symmetrize the distributions.

Figure 11. Variation of the laboratory frame light fragment anisotropies with fragment mass number.

Table I
Target Fragment Angular Distributions (mb/sr)
86 MeV/nucleon $^{12}C + ^{197}Au$

Nuclide	7°	20°	32°	44°	57°	71°	114°	133°	148°	160°
^{44m}Sc	2.21±0.12	-	0.15±0.02	0.067±0.009	0.035±0.011	0.016±0.002	0.008±0.003	0.006±0.002	0.007±0.004	0.018±0.017
^{46}Sc	2.60±0.12	0.26±0.03	0.20±0.02	0.12±0.01	0.09±0.01	0.06±0.01	0.030±0.003	0.030±0.004	0.04±0.01	0.05±0.01
^{47}Sc	-	0.055±0.052	0.048±0.03	0.050±0.005	0.044±0.010	0.033±0.014	0.005±0.001	0.023±0.005	0.025±0.003	0.041±0.007
^{48}Sc	0.28±0.23	0.59±0.16	0.13±0.05	0.064±0.024	0.044±0.018	0.034±0.007	0.021±0.003	0.023±0.004	0.017±0.007	0.023±0.007
^{52}Mn	3.36±0.13	-	0.19±0.06	0.061±0.025	0.036±0.009	0.018±0.005	0.006±0.001	-	-	0.031±0.005
^{54}Mn	17.4±0.9	0.68±0.13	0.54±0.09	0.33±0.05	0.26±0.06	0.18±0.03	0.15±0.03	0.14±0.03	0.16±0.05	0.28±0.08
^{58}Co	2.4±0.3	0.56±0.13	0.42±0.08	0.24±0.09	0.15±0.13	0.11±0.04	0.069±0.011	0.070±0.022	0.087±0.022	0.075±0.010
^{59}Fe	-	0.30±0.10	0.30±0.05	0.21±0.03	0.17±0.03	0.14±0.01	0.11±0.01	0.12±0.01	0.12±0.03	0.13±0.03
^{67}Cu	5.8±0.3	3.2±0.4	2.0±0.3	1.2±0.1	0.60±0.05	0.34±0.03	0.18±0.01	0.19±0.01	0.20±0.01	0.19±0.02
^{67}Ga	1.7±0.4	0.53±0.25	0.37±0.16	-	0.19±0.03	0.16±0.02	0.094±0.012	0.098±0.024	0.098±0.010	0.14±0.02
^{71}As	1.7±0.5	-	0.11±0.09	0.084±0.023	0.11±0.01	-	0.062±0.007	0.062±0.004	0.055±0.017	0.07±0.01
^{72}Zn	-	-	-	-	-	0.021±0.004	0.013±0.002	0.028±0.007	0.020±0.002	0.020±0.004
^{74}As	1.48±0.30	0.76±0.09	0.74±0.06	0.55±0.03	0.46±0.03	0.41±0.02	0.34±0.03	0.31±0.03	0.33±0.03	0.28±0.03
^{75}Se	3.1±0.3	0.64±0.04	0.59±0.04	0.44±0.04	0.36±0.03	0.33±0.03	0.23±0.01	0.22±0.01	0.23±0.02	0.24±0.03
^{76}As	2.9±1.2	1.68±0.42	1.12±0.26	0.85±0.17	0.45±0.07	0.36±0.04	0.23±0.04	0.24±0.04	0.21±0.05	0.22±0.10
^{77}Br	2.8±0.5	-	-	0.41±0.06	0.35±0.04	0.32±0.05	0.19±0.01	0.18±0.01	0.20±0.02	-
^{83}Sr	-	-	-	1.13±0.06	0.95±0.05	0.82±0.05	0.56±0.02	0.53±0.03	0.56±0.03	-
^{83}Rb	7.2±0.4	1.67±0.01	-	-	0.67±0.05	0.56±0.04	0.39±0.02	0.41±0.02	0.41±0.05	0.45±0.03
^{87}Y	2.8±0.1	1.53±0.45	1.43±0.07	1.08±0.04	0.92±0.03	0.78±0.04	0.53±0.02	0.51±0.02	0.52±0.03	0.52±0.02
^{88}Zr	1.1±0.5	1.67±0.08	0.66±0.06	0.54±0.03	0.46±0.04	-	0.24±0.02	0.24±0.02	0.22±0.03	0.17±0.02
^{88}Y	2.2±0.2	3.3±0.1	1.26±0.70	0.97±0.05	0.79±0.06	-	0.45±0.03	0.45±0.03	0.48±0.03	0.45±0.04
^{89}Zr	1.2±0.1	1.13±0.11	1.05±0.09	0.83±0.06	0.69±0.05	0.60±0.05	0.39±0.02	0.38±0.03	0.38±0.05	0.36±0.05
^{92m}Nb	-	1.74±0.38	0.076±0.022	0.11±0.06	0.074±0.013	-	0.038±0.006	0.027±0.003	0.013±0.002	-
^{95}Zr	-	0.30±0.07	0.29±0.06	-	0.15±0.02	0.14±0.01	0.095±0.008	0.11±0.01	0.12±0.02	0.13±0.03
^{95}Nb	0.75±0.18	0.81±0.10	0.72±0.09	0.57±0.06	0.46±0.07	0.38±0.03	0.28±0.03	0.29±0.02	0.32±0.04	0.32±0.04
^{97}Ru	1.2±0.5	-	0.63±0.10	0.36±0.05	0.30±0.03	0.23±0.01	0.14±0.01	0.12±0.01	0.12±0.01	0.12±0.04
^{99}Mo	0.87±0.57	0.38±0.14	0.36±0.12	0.25±0.04	0.21±0.02	0.18±0.01	0.13±0.01	0.14±0.01	0.16±0.02	0.17±0.02
^{101m}Rh	-	0.26±0.16	0.32±0.11	0.33±0.09	0.35±0.05	0.31±0.03	0.19±0.01	0.18±0.01	0.17±0.01	0.15±0.02
^{103}Ru	-	0.35±0.19	0.38±0.10	0.32±0.05	0.27±0.04	0.27±0.03	0.20±0.02	0.26±0.02	0.21±0.02	0.24±0.02
^{105}Rh	-	-	0.48±0.18	0.33±0.19	0.26±0.11	0.33±0.04	0.20±0.03	0.22±0.03	0.19±0.05	0.17±0.10
^{106m}Ag	-	-	0.25±0.05	0.20±0.02	0.15±0.02	0.15±0.01	0.091±0.004	0.088±0.006	0.08±0.01	0.08±0.012
^{111}In	-	0.51±0.08	-	0.38±0.04	0.32±0.02	0.27±0.01	0.15±0.01	0.126±0.006	0.117±0.006	0.106±0.015
^{117m}Sn	-	-	0.078±0.033	0.078±0.007	0.080±0.010	0.082±0.014	0.056±0.008	0.016±0.007	0.052±0.005	-
^{121}Te	0.63±0.19	0.63±0.11	0.51±0.10	0.41±0.05	-	0.29±0.04	0.13±0.01	0.089±0.016	0.099±0.019	0.07±0.02
^{121m}Te	-	-	-	-	-	0.080±0.026	0.043±0.009	0.036±0.008	0.047±0.012	-
^{127}Xe	-	0.77±0.07	0.75±0.06	-	0.045±0.007	0.023±0.009	0.009±0.003	-	0.09±0.01	0.093±0.027
^{128}Ba	-	-	0.30±0.14	0.28±0.08	0.25±0.03	0.17±0.02	0.059±0.016	0.048±0.023	-	-

Nuclide	7°	20°	32°	44°	57°	71°	114°	133°	148°	160°
^{131}Ba	-	0.77±0.15	1.98±0.17	0.98±0.09	0.72±0.05	0.44±0.01	0.16±0.01	0.13±0.01	0.097±0.014	0.086±0.056
^{137}Cs	-	1.67±0.54	0.99±0.39	-	0.40±0.16	0.46±0.16	0.27±0.06	0.23±0.07	0.75±0.07	1.03±0.25
^{139}Ce	-	1.73±0.21	1.54±0.11	0.55±0.06	0.29±0.02	-	0.081±0.006	0.062±0.009	-	-
^{145}Eu	7.0±0.4	6.0±0.3	-	2.14±0.07	1.01±0.07	0.42±0.03	0.085±0.012	0.09±0.01	0.061±0.011	0.060±0.009
^{146}Gd	8.9±0.6	5.8±0.2	3.3±0.2	2.3±0.2	1.05±0.05	0.48±0.05	0.039±0.002	0.047±0.007	0.055±0.001	0.075±0.024
^{147}Eu	11.6±2.1	5.3±0.3	1.81±0.01	2.1±0.1	0.69±0.05	0.37±0.07	0.16±0.02	0.46±0.06	0.068±0.026	0.17±0.04
^{147}Gd	3.1±0.7	6.0±0.6	4.6±0.1	1.6±0.2	0.85±0.11	0.41±0.26	0.097±0.063	0.075±0.008	-	-
^{149}Gd	10.8±0.7	9.5±0.2	5.4±0.2	2.4±0.1	1.05±0.04	0.36±0.05	0.056±0.004	0.055±0.007	0.043±0.009	-
^{152}Tb	-	5.7±0.4	3.2±1.0	1.2±0.5	0.37±0.13	-	-	-	-	-
^{153}Tb	4.4±0.1	4.1±0.1	4.0±0.3	2.5±0.3	0.74±0.05	0.38±0.05	0.017±0.005	-	0.036±0.009	-
^{153}Gd	6.8±1.7	5.8±0.5	-	1.3±0.2	0.69±0.14	0.19±0.07	-	-	-	-
^{153}Sm	-	1.15±0.25	0.72±0.11	0.28±0.06	0.15±0.09	-	-	-	-	-
^{155}Tb	14.7±1.0	13.0±0.6	8.1±1.4	2.98±0.03	1.16±0.06	0.42±0.03	0.064±0.007	0.069±0.01	0.06±0.02	-
^{160}Er	15.8±0.5	8.9±0.6	5.0±0.5	2.44±0.07	0.99±0.14	0.60±0.08	-	0.026±0.010	-	-
^{165}Tm	26.9±2.6	18.5±1.0	14.6±0.7	4.4±0.5	-	0.58±0.01	-	-	-	-
^{166}Yb	5.5±1.1	15.0±0.3	11.0±0.5	4.9±0.2	1.59±0.11	0.62±0.07	0.68±0.06	0.11±0.04	0.64±0.07	0.73±0.08
^{167}Tm	30.3±1.4	23.5±0.6	13.1±0.5	5.6±0.3	2.19±0.10	0.68±0.06	0.072±0.007	0.11±0.01	0.08±0.01	0.11±0.01
^{169}Yb	18.8±0.7	14.1±0.4	8.3±0.4	6.2±0.1	1.36±0.06	0.38±0.03	0.045±0.005	0.066±0.007	0.069±0.007	-
^{169}Lu	17.5±2.9	11.7±0.9	6.9±0.7	3.1±0.4	1.62±0.11	0.49±0.08	0.048±0.021	0.12±0.01	-	-
^{170}Lu	28.3±1.8	21.7±1.3	14.0±1.3	6.7±0.7	2.44±0.24	0.72±0.16	-	-	-	-
^{170}Hf	-	18.0±0.9	9.5±0.4	5.4±0.3	1.98±0.60	0.63±0.49	-	-	-	-
^{171}Lu	20.7±0.6	15.9±0.4	8.8±0.1	4.4±0.1	1.72±0.07	0.56±0.03	0.08±0.01	-	0.075±0.019	0.092±0.013
^{173}Hf	38.0±2.9	20.2±0.8	14.1±0.7	5.7±0.4	3.11±0.42	0.72±0.02	0.069±0.015	0.11±0.02	0.10±0.01	0.09±0.03
^{175}Hf	26.9±1.5	20.1±0.6	12.8±0.4	6.2±0.3	3.13±0.06	0.85±0.06	1.15±0.02	0.12±0.01	0.11±0.02	-
^{175}Ta	21.5±7.4	16.3±0.9	11.0±0.7	-	0.46±0.09	0.71±0.26	-	0.15±0.03	-	-
^{181}Re	29.2±7.7	18.6±0.8	12.5±0.8	8.5±0.4	3.78±0.01	-	0.11±0.03	0.21±0.07	2.1±0.1	-
^{187}Hf	15.2±4.7	9.2±1.6	-	2.7±0.2	1.12±0.30	-	-	-	-	-
^{182}Os	30±12	18.8±2.4	14.4±1.3	9.2±1.4	4.0±0.5	1.77±0.56	-	-	-	-
^{185}Os	22.7±1.0	19.0±0.6	14.0±0.5	8.4±0.3	3.9±0.1	1.31±0.08	0.11±0.02	0.20±0.03	-	0.12±0.04
^{188}Pt	19.7±1.0	18.6±0.5	16.5±0.3	7.9±0.2	4.2±0.1	1.09±0.04	0.08±0.01	0.16±0.01	0.10±0.02	0.16±0.04
^{189}Ir	16.9±4.0	-	11.5±1.0	6.2±0.8	2.8±0.3	1.05±0.08	0.10±0.04	0.20±0.05	-	-
^{191}Pt	46.4±4.4	23.5±1.4	21.9±0.2	13.3±0.9	6.5±0.4	0.28±0.26	0.40±0.10	0.71±0.11	1.2±0.3	-
^{194}Au	149±42	7.9±0.5	7.1±0.4	6.3±0.4	3.1±0.2	1.25±0.07	0.20±0.03	0.21±0.01	0.34±0.06	0.56±0.08
^{196}Au	26.4±3.9	5.4±0.1	5.3±0.1	4.6±0.2	2.9±0.1	2.6±0.1	0.64±0.01	0.66±0.01	1.78±0.03	2.29±0.01

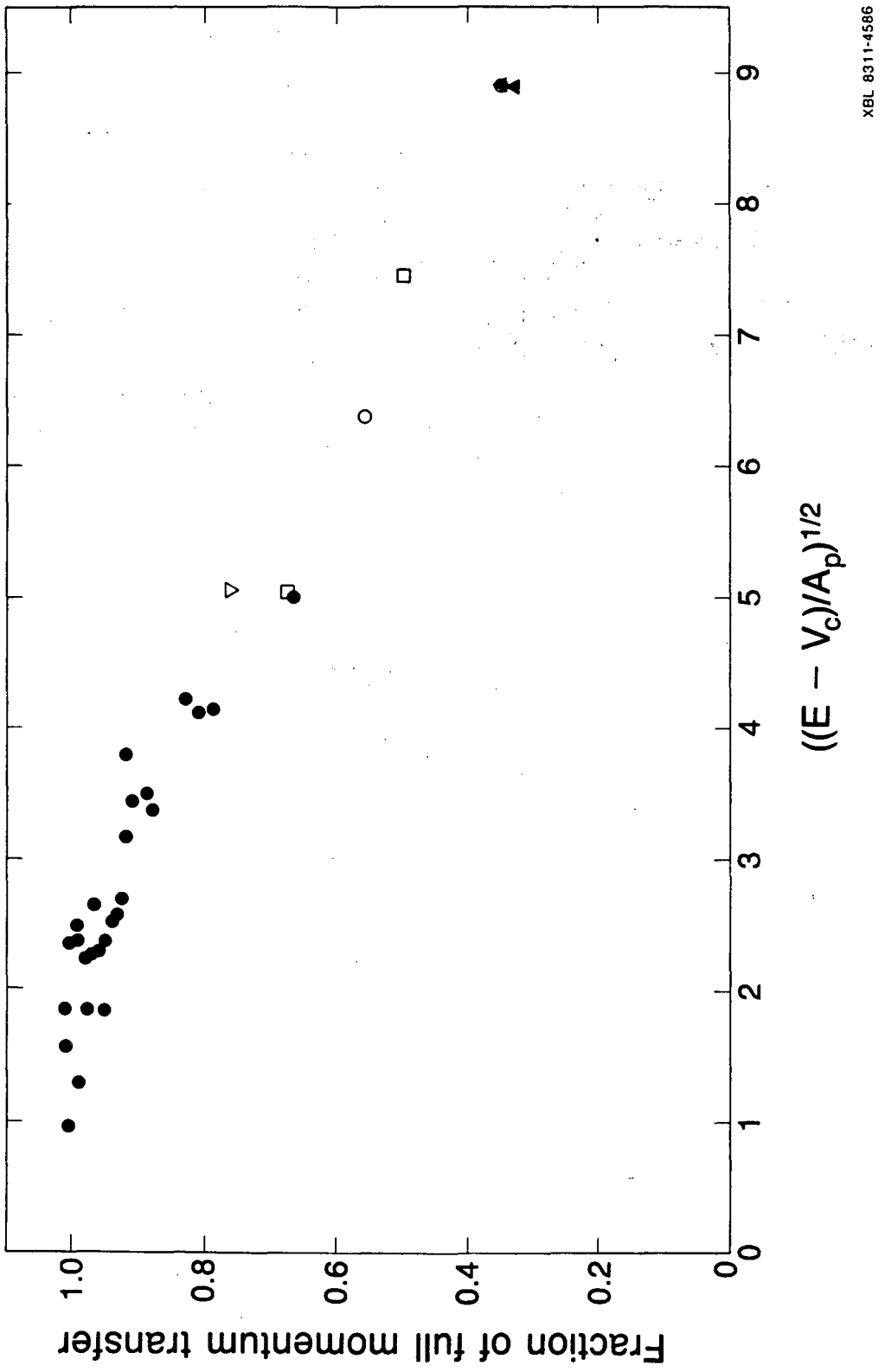
Fraction of full momentum transfer
1.0
0.8
0.6
0.4
0.2
0
0
1
2
3
4
5
6
7
8
9
$((E - V_c)/A_p)^{1/2}$
XBL 8311-4586

Figure 1

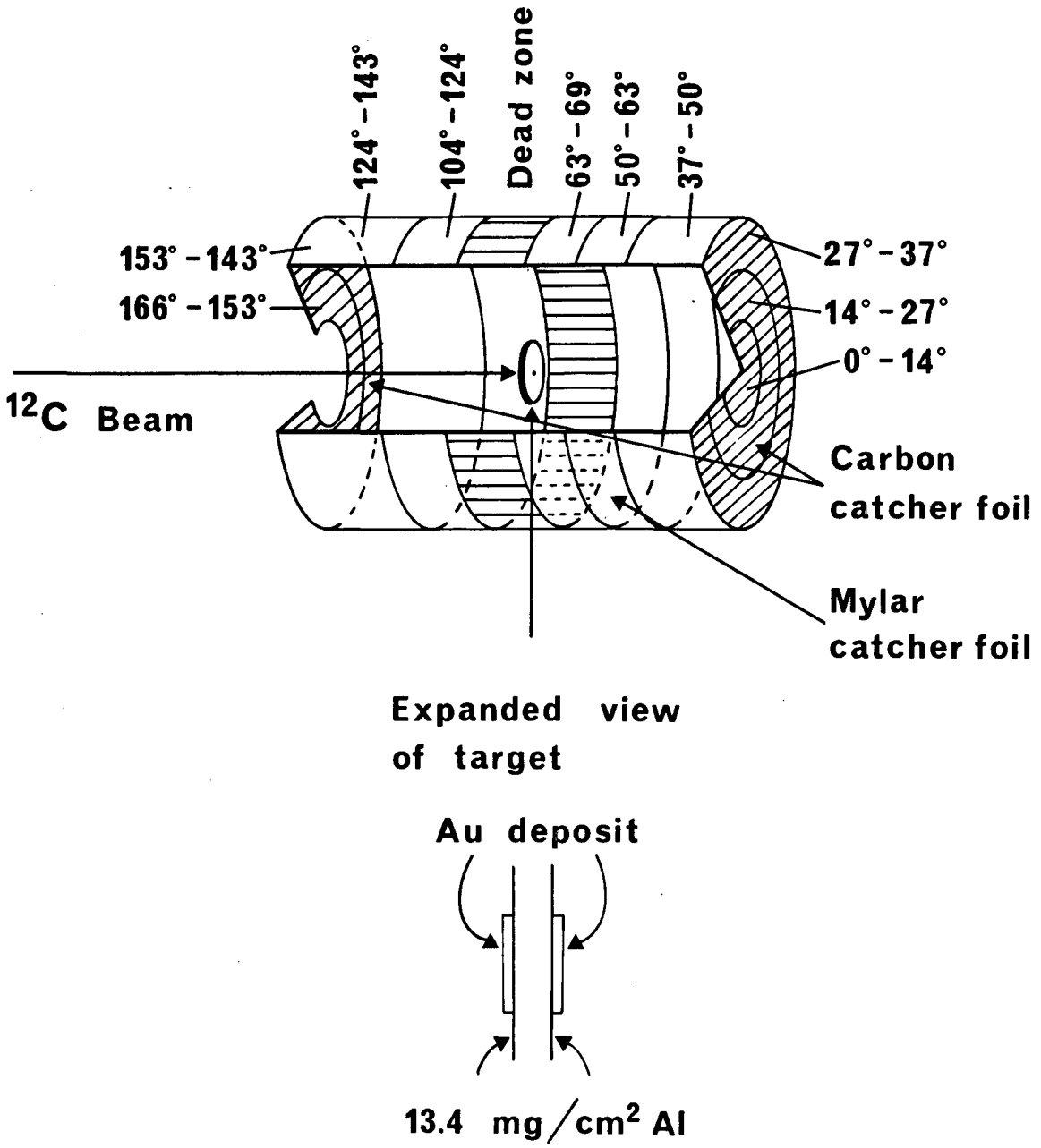

XBL 8312-2481

Figure 2

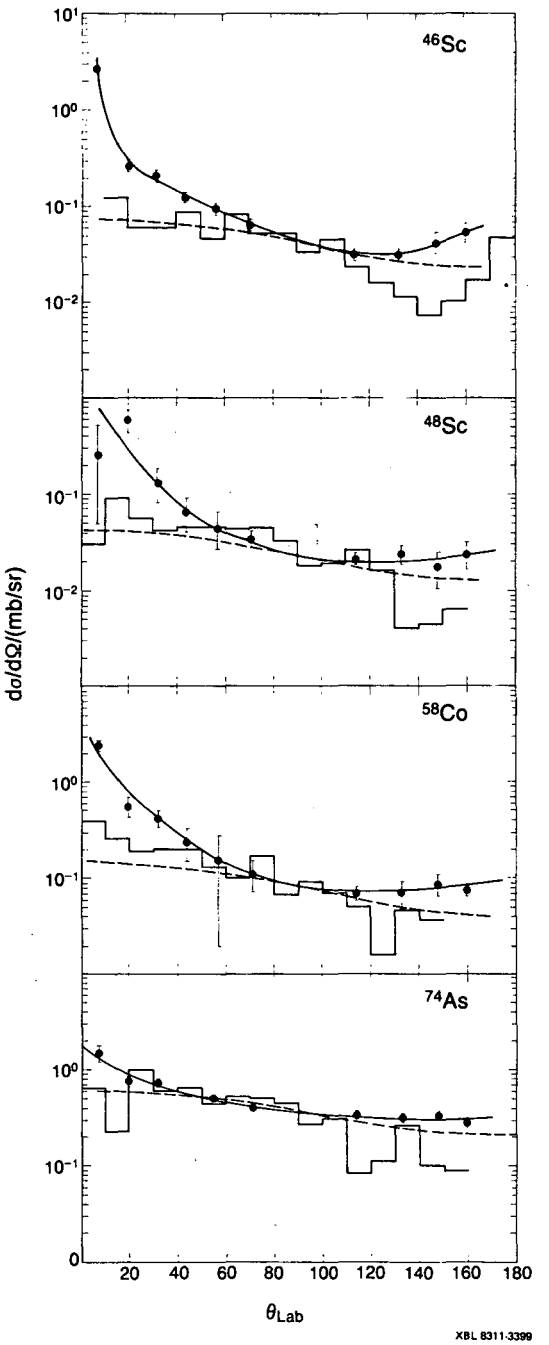

Figure 3

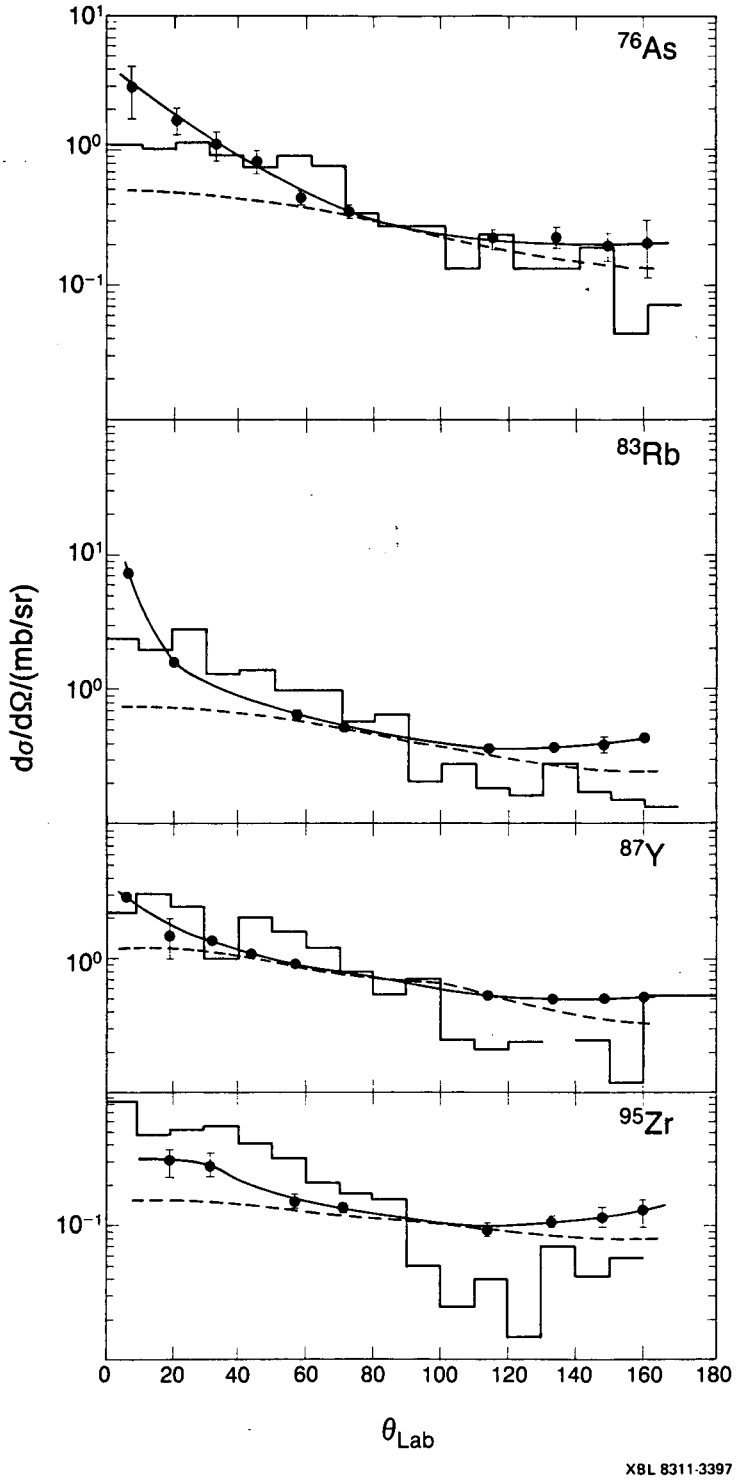
^{76}As
^{83}Rb
^{87}Y
^{95}Zr
10^1
10^0
10^{-1}
$d\sigma/d\Omega/(mb/sr)$
0
20
40
60
80
100
120
140
160
180
θ_{Lab}
XBL 8311-3397

Figure 4

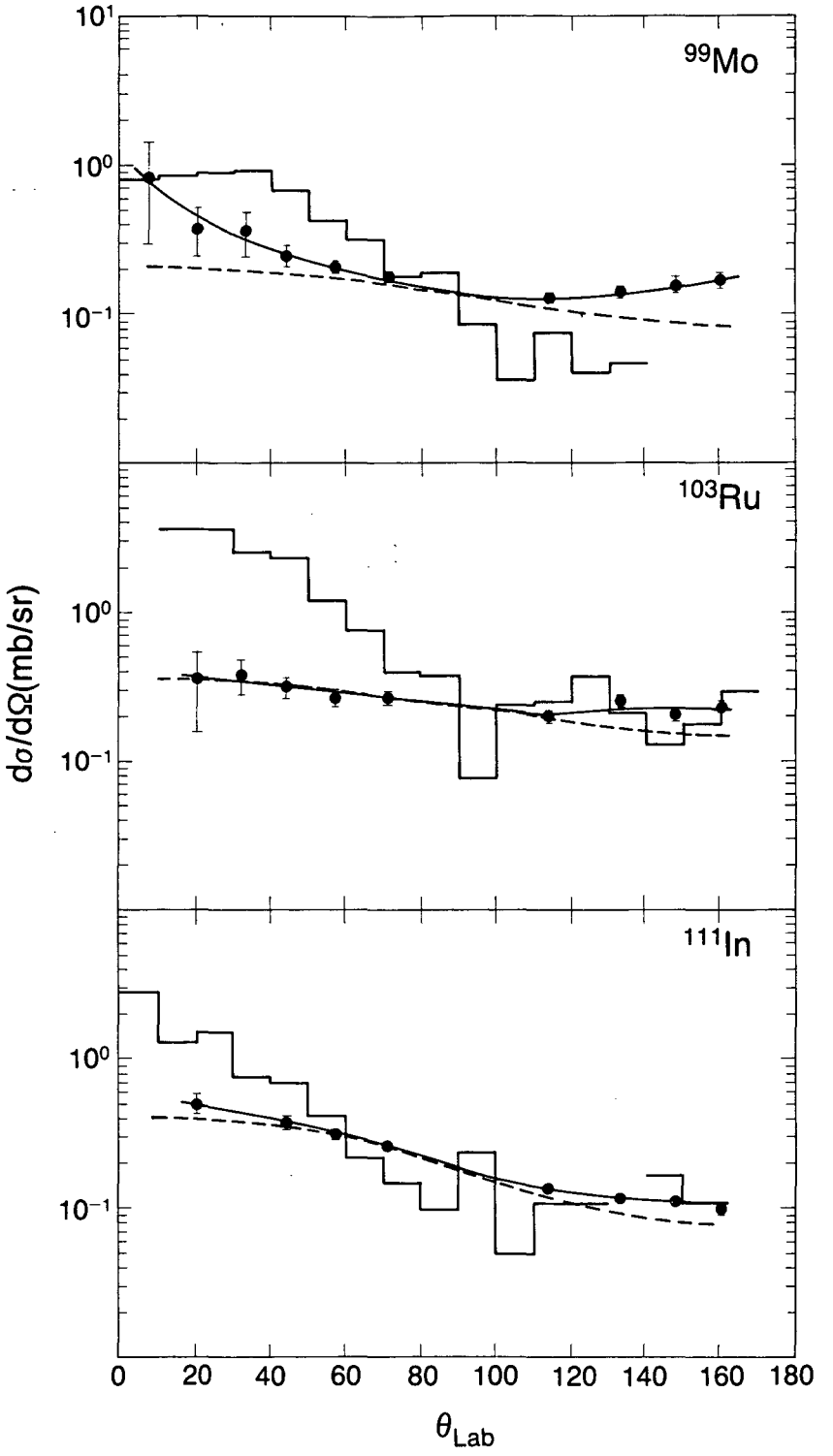
10^1
10^0
10^{-1}
^{99}Mo
^{103}Ru
^{111}In
dσ/dΩ(mb/sr)
0
20
40
60
80
100
120
140
160
180
θ_{Lab}
XBL 8311-4583

Figure 5

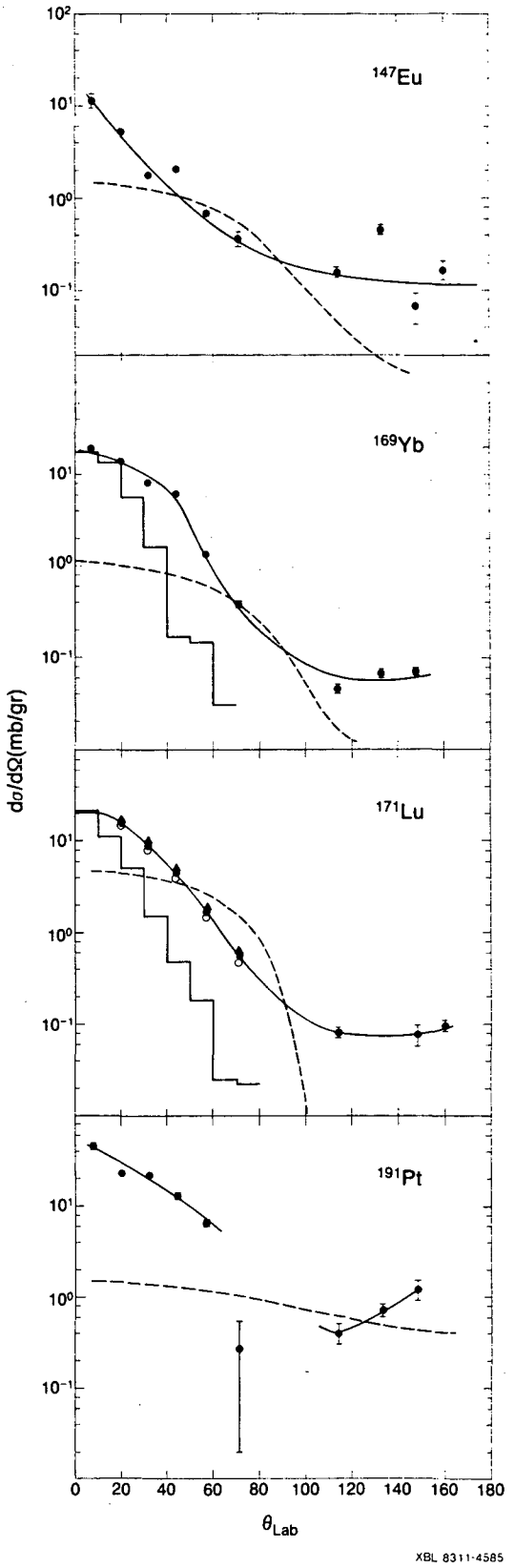

Figure 6

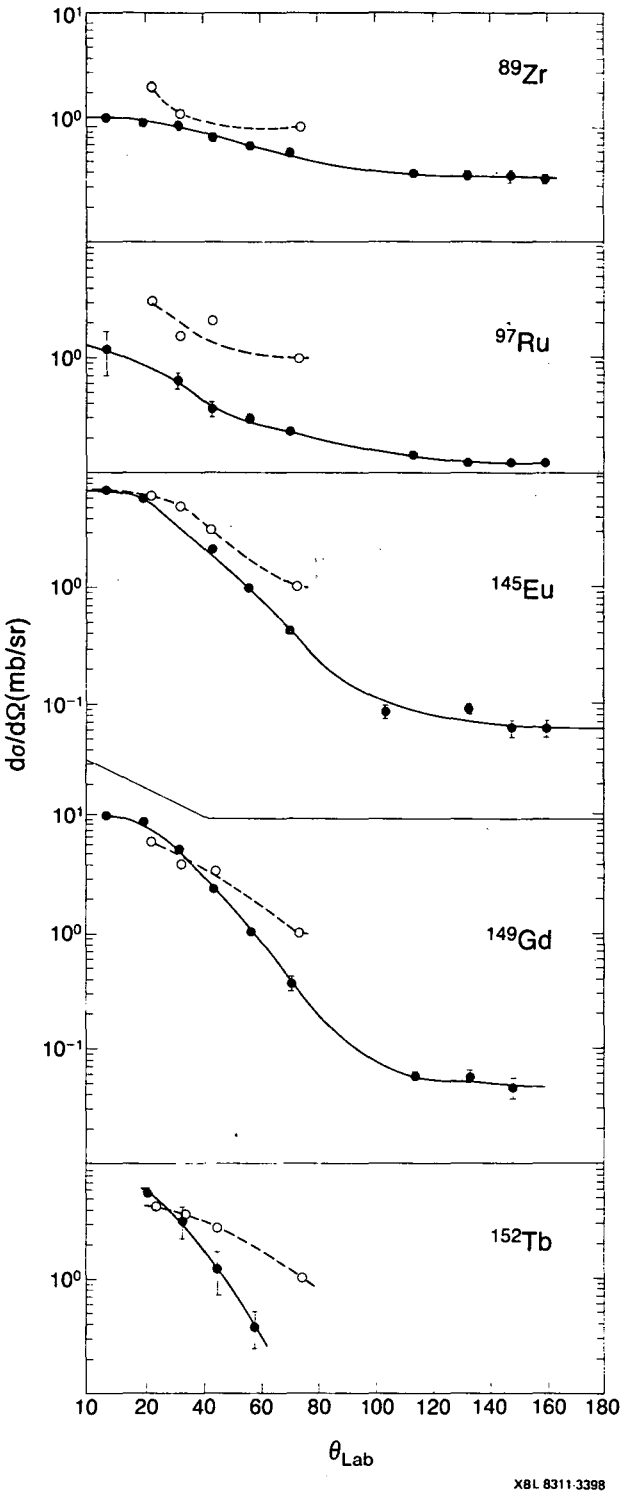
^{89}Zr
^{97}Ru
^{145}Eu
^{149}Gd
^{152}Tb
dσ/dΩ(mb/sr)
θ_{Lab}
X8L 8311-3398

Figure 7

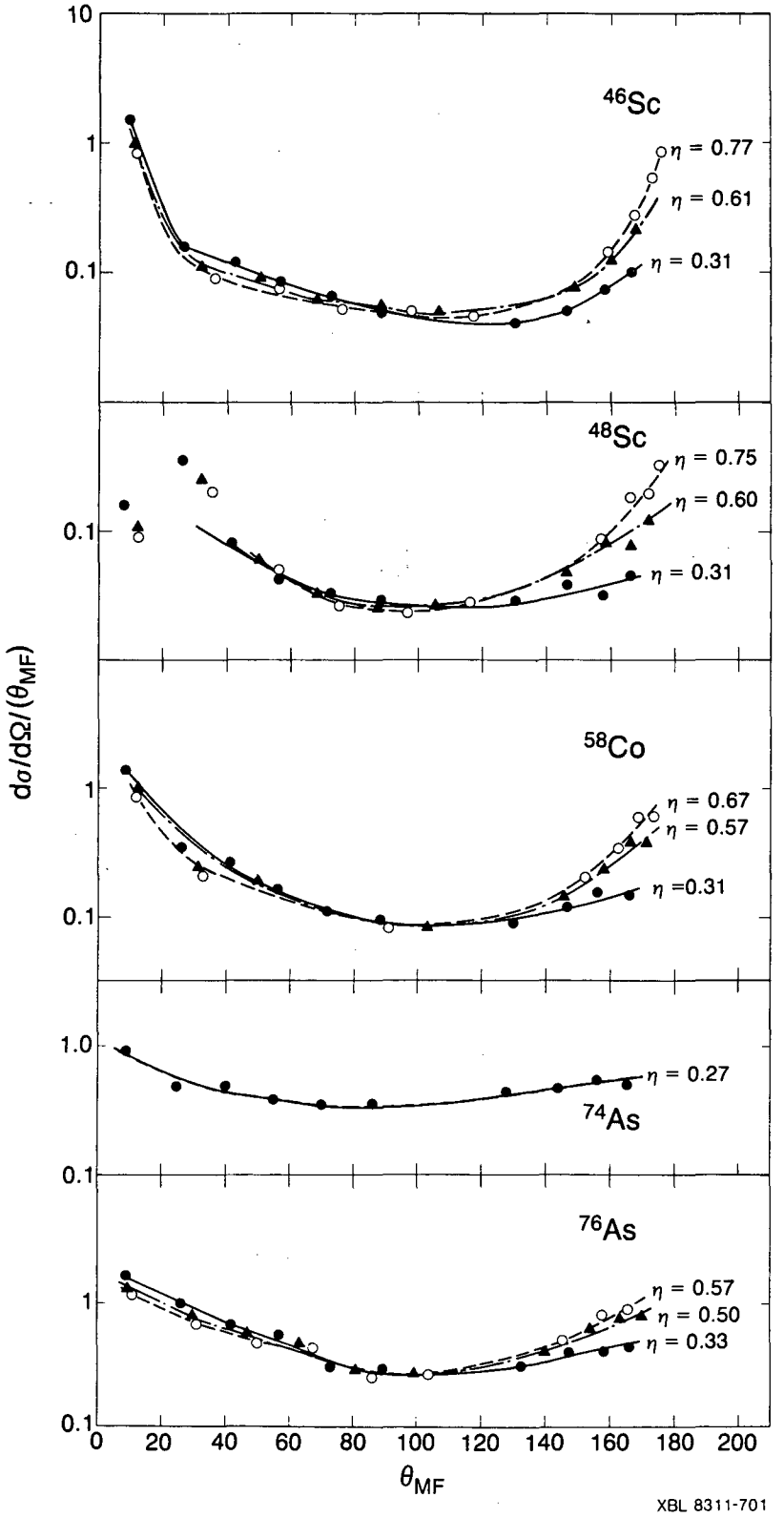
^{46}Sc
η = 0.77
η = 0.61
η = 0.31
^{48}Sc
η = 0.75
η = 0.60
η = 0.31
^{58}Co
η = 0.67
η = 0.57
η =0.31
η = 0.27
^{74}As
^{76}As
η = 0.57
η = 0.50
η = 0.33
dσ/dΩ/(θ$_{MF}$)
θ$_{MF}$
XBL 8311-701

Figure 8

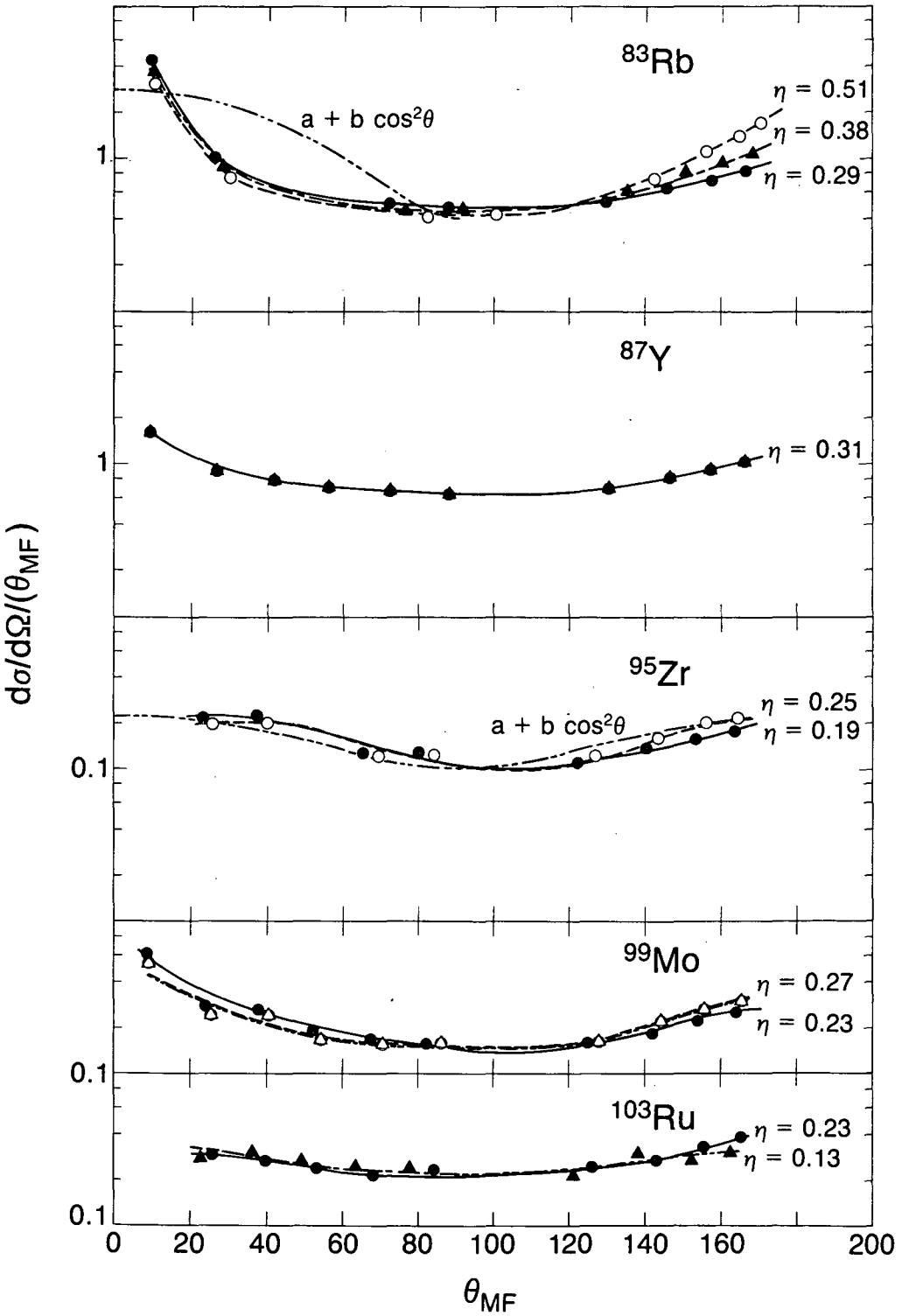

XBL 8311-4584

Figure 9

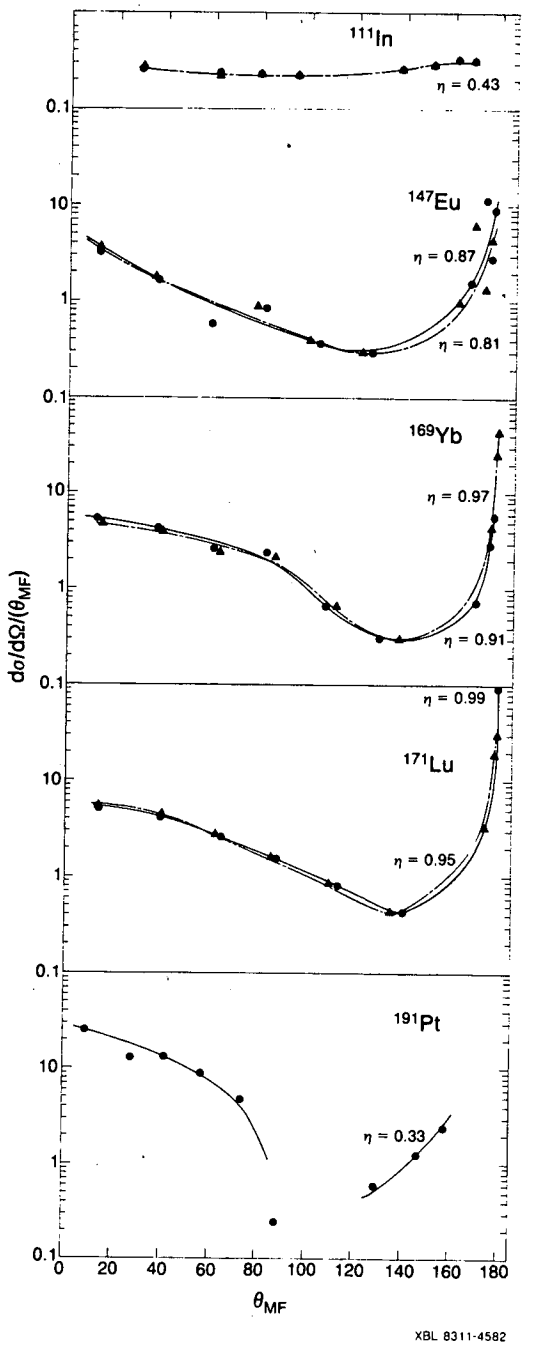
^{111}In
η = 0.43
^{147}Eu
η = 0.87
η = 0.81
^{169}Yb
η = 0.97
η = 0.91
η = 0.99
^{171}Lu
η = 0.95
^{191}Pt
η = 0.33
dσ/dΩ/(θ$_{MF}$)
θ$_{MF}$
XBL 8311-4582

Figure 10

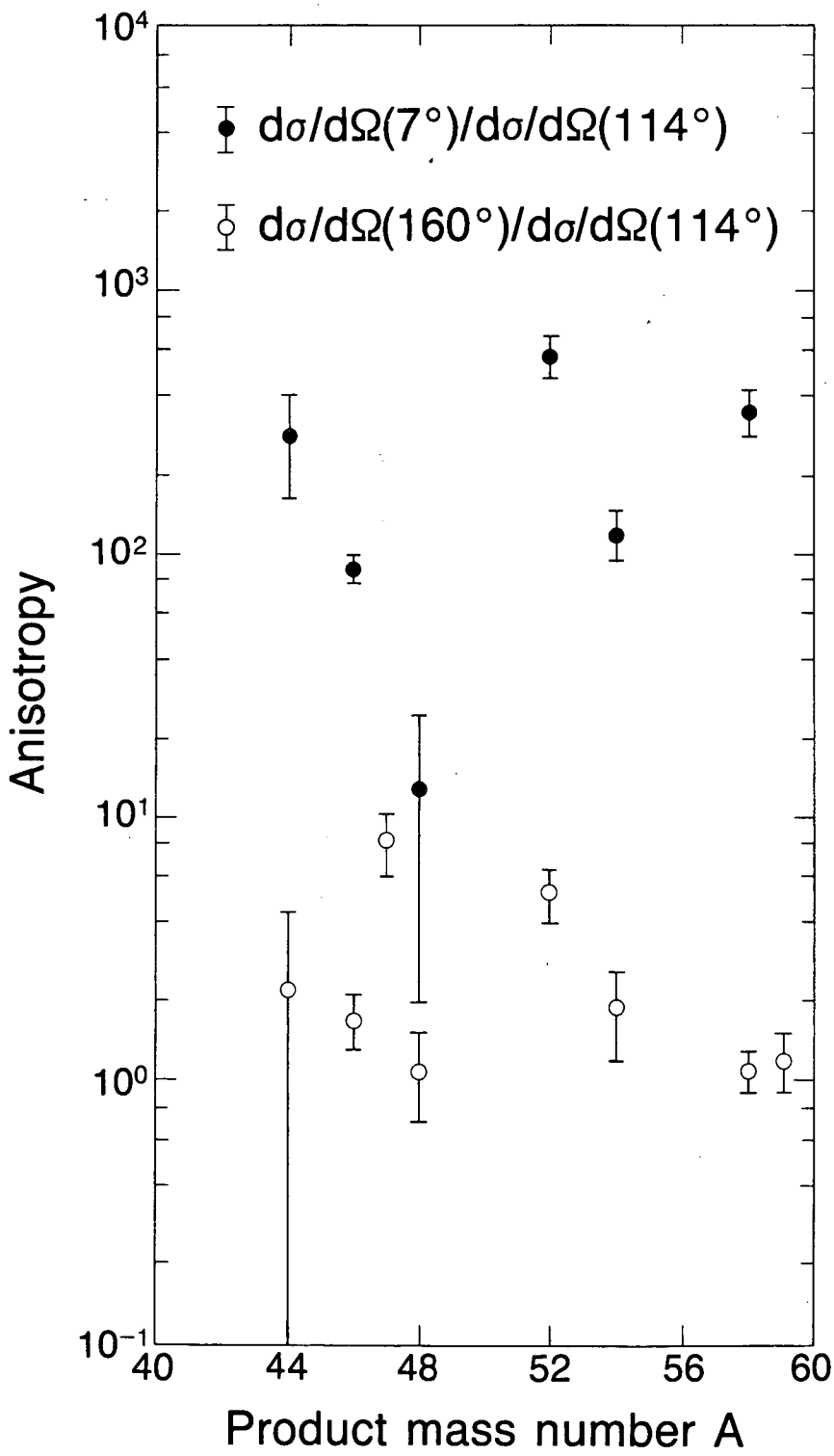

XBL 8311-4587

Figure 11

This report was done with support from the Department of Energy. Any conclusions or opinions expressed in this report represent solely those of the author(s) and not necessarily those of The Regents of the University of California, the Lawrence Berkeley Laboratory or the Department of Energy.

Reference to a company or product name does not imply approval or recommendation of the product by the University of California or the U.S. Department of Energy to the exclusion of others that may be suitable.

TECHNICAL INFORMATION DEPARTMENT
LAWRENCE BERKELEY LABORATORY
UNIVERSITY OF CALIFORNIA
BERKELEY, CALIFORNIA 94720